V1D1: An electrostatic Vlasov Simulation Code

Clare E. J. Watt

July 20, 2011

Technical Guide to V1D1

1 Introduction

The V1D1 simulation code is a one-dimensional numerical model of electrostatic waves which can be driven unstable by the presence of finite currents or beam distributions. The simulation uses periodic boundary conditions in configuration space to model an idealised plasma instability. The user supplies the plasma properties, and obtains a full range of diagnostics, from the solutions to the linear dispersion relation to the full particle distribution functions. Many electrostatic instabilities in a magnetic field-free plasma can be simulated with this numerical code (see e.g. Chapter 3 in S. P. Gary, *Theory of Space Plasma Microinstabilies* [2003] for examples).

In the spirit of the International School for Space Simulations (ISSS), this code is presented for tutorial purposes. It has been used for scientific analysis (e.g. Watt et al., *GRL* [2002]), but there are many more sophisticated Vlasov simulations in use around the world, as some of the presentations at ISSS-10 will demonstrate! I hope that it will provide some help for researchers who are developing their own simulations from scratch.

Appended to the end of this document is a chapter from my Ph.D. thesis which explains the governing equations and algorithms used in the simulation. In the next couple of sections, I will explain the layout of the source code and how to use it.

2 Source Code

The source code for V1D1 has two parts. The first part (`v1d1`) sets up the simulation grid according to the expected range of growing waves obtained from solutions to the linear dispersion relation. The second part (`v1d1sim`) performs the electrostatic simulation.

2.1 Intro to `v1d1`

The program `v1d1` uses the user-supplied input information and calculates solutions to the linear electrostatic dispersion relation to identify wavenumbers over which waves will grow most strongly. This information is used to construct a grid in real space for the simulation. The temperature and drift speed information supplied by the user is used to construct a velocity grid for each plasma species which covers the full distribution function. The phase velocity information from the linear dispersion relation solutions is also used to construct the resolution of the velocity space grids. The Courant condition gives the timestep. Distribution functions are constructed from a sum of Maxwellian components. Each component should be fully specified in the input file. If information about the protons is not provided, then it assumed that they are stationary.

2.2 Source code for `v1d1`

The source code for `v1d1` is written in Fortran90 and can be found in the file *v1d1code.f90*. For portability, I have tried to use standard fortran and to limit the use of libraries. If you have problems compiling it on your home machine, please let me know.

The code uses two modules: *nrtype* defines the fortran types and *parameters* contains physical parameters and unit numbers for input and output files.

The program is called *iaisetup* for 'historical' reasons; it was originally used to simulation current-driven ion acoustic instabilities, and because it sets up the simulation grid. The main branching `if` statement (line 337) chooses a different path depending on whether a proton component has been specified or not.

The subroutine *newton* solves the dispersion relation given physical parameters, a wavenumber and an initial guess at the solution.

The other subroutines in the file are required by the *newton* subroutine.

2.3 Input/Output for `v1d1`

`v1d1` takes input file `aaaaa.in` (please ensure there are five - and only five - characters in the filename!) and uses the information in it to generate the output files `aaaaa.out` and `aaaaa.dr.dat`. The code has been developed so that it might include more options in the future, not all of them are available in its present incarnation.

The input file must follow a particular format, which includes the spacing indicated below:

```
2                       ncomps: number of plasma components

1                       species: 1=electron, 2=proton
maxwellian              form: form of distribution function 1
1.0e+06                 nden: number density (m^-3)
2.0                     temp: temperature (eV)
0.0e+00                 drift: drift velocity (m/s)
```

```
1                       species: 1=electron, 2=proton
maxwellian              form: form of distribution function 2
1.0e+05                 nden: number density (m^-3)
1.0                     temp: temperature (eV)
2.5e+06                 drift: drift velocity (m/s)

6.0                     mvth: multiple of largest thermal speed for vcut
0.8                     cf: Courant Factor
100000                  ntmax: max no. of timesteps
10000                   fwrite: how often f is saved
1000                    ewrite: how often e is saved
```

This example is for an electron beam instablity, where the ion motion is ignored.

The text from lines 3-8 (including the blank line 8) should be repeated `ncomps` times. The only form of the distribution function that this code accepts is the `maxwellian` form.

Plasma properties are to be given in physical units. This may involve some off-line calculations, especially for drift speeds etc. The parameter `vcut` is the highest velocity in the velocity grid and is calculated in the `v1d1` program. The variable `mvth` ("multiple of thermal speed") can be altered by the user. Generally, `mvth`> 4 is recommended.

The maximum number of timesteps is the only grid parameter that the user has full control over. This parameter is often best obtained iteratively. The output file `aaaaa.out` informs the user how long the simulation will run (in electron plasma periods) and so the `ntmax` parameter can be adjusted after `v1d1` has been run once to achieve the runtime you want. Note that if you change `ntmax` you should then re-run `v1d1`!

Since the full two-dimensional distribution function can be very large, `fwrite` and `ewrite` give you the option to output a smaller volume of diagnostics more often. `fwrite` controls how often the full distribution functions are written to file (i.e. every `ewrite` timesteps), and `ewrite` controls how often the electric field, plasma moments, spatially-averaged distribution functions and other simulation diagnostics are written. We recommend that `fwrite` is a multiple of `ewrite` so that you may study all diagnostics at the same time.

The output file (`aaaaa.out`) contains grid information:

```
 THE INPUT PARAMETERS ARE

maxwellian      form of component  1
Number density, temperature and drift
 1.0000E+06
 2.0000E+00
```

```
 0.0000E+00

maxwellian      form of component  2
Number density, temperature and drift
 1.0000E+05
 1.0000E+00
 2.5000E+06

 6.000          mvth: multiple of thermal speed for vcut
 0.800          cf: courant factor
 8.4772E-06     enoise: Initial e-field perturbation amplitude

 PLASMA DIAGNOSTICS
 8.3877E+05     ae: Electron thermal speed (main bulk component)
 0.0000E+00     ai: Ion thermal speed (main bulk component)
 5.9168E+04     wpe: Electron plasma frequency
 1.3808E+03     wpi: Ion plasma frequency
    10.0239     debye: Debye length (using electron temperature)
 1.3841E+04     cs: Ion acoustic speed

 INFORMATION ABOUT UNSTABLE WAVES
 1.2765E-03     kmin: The smallest value of unstable k
 4.9511E-02     kmax: The largest value of unstable k
 1.2690E+02     lmin: The shortest wavelength
 2.4611E+03     lmax: The longest wavelength
The length of the box is such that it can hold the longest
wavelength
 1.6520E+06     vphmin: The phase velocity at kmin
 2.3188E+06     vphmax: The phase velocity at kmax
 9.0681E+03     maxgamma: The maximum value of gamma

 GRID DIMENSIONS
 2.4611E+03     Lx: box size in x, in m
 7.5347E+06     vcute: box size in vx for electrons, in m/s
    10.0239     dx: stepsize in x, in m
 6.6678E+04     dve: stepsize in vx for electrons, in m/s
 1.1028E-08     dt: timestep, in s
   246          nx: number of spatial grid points
   113          envx: number of ve points
 100000         ntmax: number of timesteps
 6.5249E+01     phystime: total simulation time in 1/wpe
 100000
 Run has been completed successfully
```

Input information is repeated for cross-checking purposes (you can ensure

that the grid setup program you ran matched the simulation). You do not have to manually alter this file, it is transferred directly to the simulation program. Note that the information about unstable waves is in SI units (respectively m^{-1}, m, m/s and s^{-1}).

This example is for an electron beam instablity, where the ion motion is ignored. When an ion component is included, there are more lines toward the end of the file to include the ion velocity grid information. Note that all parameters share the same grid in real space (x). The velocity grid stretches from $-v_{cut,e}$ to $+v_{cut,e}$. The integer `envx` gives the number of grid points in the positive velocity direction between $v_x = 0$ and $v_x = v_{cut,e}$ and so the full number of electron velocity gridpoints is $2\times$ `envx` $+1$. The timestep for electrostatic instabilities tends to be very small.

Note that the last two lines of `aaaaa.out` are not added until the simulation has been run. The second last line keeps track of the last time the simulation electric field output was recorded (in case the simulation stops unexpectedly), and the last line is only added if the simulation reaches `ntmax` timesteps. Note that the simulation is not infinitely stable - eventually the distribution function may develop structure that is too fine for the grid to handle, or the electric field amplitude may become larger than initially anticipated. This does not necessarily mean that the simulation output is un-usable, and it is worth checking the output in these circumstances to see why the simulation stopped.

The file `aaaaa.dr.dat` contains the solutions to the linear dispersion relation which were used to calculate the simulation grid. The data is provided in three columns which contain the wavenumber k_x in m^{-1}, the real part of the frequency ω_r in rad/s, and the imaginary part of the frequency γ in rad/s.

The file `aaaaa.xcoord.dat` contains the x-coordinates of the real space grid to be used in the simulation. The files `aaaaa.evcoord.dat` and `aaaaa.ivcoord.dat` contain the velocity grid coordinates for the electron and proton velocity grids respectively.

2.4 Intro to `v1d1sim`

The `v1d1sim` program runs the simulation. It takes the information from the `aaaaa.out` file and constructs the simulation grids, distribution functions and noisy background electric field. These initial conditions drive the simulation.

2.5 Source code for `v1d1sim`

The source code for `v1d1sim` is written in Fortran90 and can be found in the file *v1d1simcode.f90*. For portability, I have tried to use standard fortran and to limit the use of libraries. If you have problems compiling it on your home machine, please let me know.

The code uses the same two modules as `v1d1`.

The program is called *iaisim* for 'historical' reasons; it was originally used to simulation current-driven ion acoustic instabilities, and because it is the simulation part of the model. The main branching `if` statement (line 296)

chooses a different path depending on whether a proton component has been specified or not.

There are many more subroutines in `v1d1sim`. The subroutine *initf* initialises the distribution functions and the noisy electric field. All subroutines titled *subroutine_e* are the equivalent subroutines for 'electron-only' simulations where the ions are stationary.

The *mccorm* subroutine performs the most work in the simulation, since it is responsible for the time integration of the Vlasov equation using the MacCormack algorithm. Boundary conditions are applied directly in this subroutine. Periodic boundary conditions are applied in the spatial direction. The points at the boundary in velocity space are integrated forward in time by applying a fourth-order one-sided finite difference for the velocity derivative which appears in the Vlasov equation.

The *inpairs* subroutine calculates the integrals of the distribution function to obtain the moments. The first moment is used to construct the current density which drives the electric field perturbations.

The *entropy* subroutine calculates the entropy in the simulation. This is useful for a simulation diagnostic (see thesis Chapter 3).

The subroutine *wrdata* is responsible for simulation output. There are many simulation diagnostics in different output files, please see the next section for details.

The subroutine *f1check* is provided so that the simulation halts gracefully when perturbations in the distribution function become too large.

2.6 Input/Output for `v1d1sim`

The input for the simulation is the `aaaaa.out` file supplied by `v1d1`. The output files generated by `v1d1sim` are numerous, but are constructed so that post-processing of the simulation data can be kept at a minimum. Plasma moments etc are already calculated in the program, therefore it is more efficient to output these as the simulation is running.

File	Columns	Variable(s)	Contents
`aaaaa.dia.dat`	4	Diagnostics	K_e, K_i, I_e, entropy
`aaaaa.exx.dat`	3	Electric field	x, t, E_x
`aaaaa.fe0.dat`	3	Spatially-averaged f_e	v_x, t, f_{e0}
`aaaaa.fi0.dat`	3	Spatially-averaged f_i	v_x, t, f_{i0}
`aaaaa.jxx.dat`	3	Current density	x, t, J_x
`aaaaa.nex.dat`	3	Electron number density	x, t, n_e
`aaaaa.nix.dat`	3	Proton number density	x, t, n_i
`aaaaa.res.dat`	1	Anomalous resistivity	η
`aaaaa.rho.dat`	3	Charge density	x, t, ρ
`aaaaa.tex.dat`	3	Electron temperature	x, t, T_e
`aaaaa.tix.dat`	3	Proton temperature	x, t, T_i
`aaaaa.uex.dat`	3	Electron drift velocity	x, t, u_e
`aaaaa.uix.dat`	3	Proton drift velocity	x, t, u_i

Please see the chapter at the end of this document for definitions of the physical parameters.

Files `aaaaa.fex.dat` and `aaaaa.fix.dat` are large single column files containing snapshots of the full distribution functions. The data is ordered first in the spatial direction, then in the velocity direction and then in time. For example, if there is only one snapshot in the file, then the data is organised:

```
f(x=0,vx=-vcut)
f(x=1,vx=-vcut)
f(x=2,vx=-vcut)
...
f(x=0,vx=-vcut+1)
f(x=1,vx=-vcut+1)
f(x=2,vx=-vcut+1)
...
etc
...
f(nx-1,vx=+vcut)
f(nx,vx=+vcut)
```

There will be a total of $NX \times (2 * ENVX + 1)$ entries for each snapshot. Visualisation of the full distribution function is best done using surface or contour plots.

You can inadvertently generate huge files by using a small fwrite parameter - be careful!

3 Running Instructions

All the programs are run from a linux command line. Here is how I recommend that you run the model:

1. Create a new directory for your new run
2. Change the `aaaaa.in` file parameters
3. Type `make` to ensure that the executable file is up-to-date
4. Type `./v1d1.x` and enter, you will be prompted for the input filename
5. Type full input filename (including the .in suffix)
6. Open `aaaaa.out` file to check simulation grid parameters - does it seem reasonable? That is, are any parameters NaN or 0? (note that some proton parameters are zero if it's an 'electrons-only' simulation run). Note also that if any of the grid sizes is > 500 points then the program will take a long time to run.

7. Keep changing `aaaaa.in` and running `v1d1.x` until you are satisfied.

8. Type `./v1d1sim.x` and enter, you will be prompted for the input filename - CAREFUL! This time it's `aaaaa.out`!

Inevitably, you will find input parameters which do not generate growing waves, or which give nonsensical grids. The set-up routine `v1d1` is not foolproof. You must ensure that you check `aaaaa.out` before running `v1d1sim`.

4 Some Troubleshooting Suggestions

The root-finding algorithm in `v1d1` may not find any roots - an error message will appear on your screen telling you that no root has been found. In this case, you can change the initial guess and try to find some solutions (line 353 for proton/electron simulations and line 570 for electron-only simulations).

If insufficient wavenumbers have been analysed, `v1d1` will stop with the message 'still growing solutions at nmax'. The parameter `nmax` controls how many wavenumbers are studied and can be changed on line 169. Note that the easiest way to ensure that roots are found is to move through wavenumber space very gradually, using the previous solution to provide the guess for the next one. You can also change the wavenumber increment in lines 351 and 568 if you want to extend the range of wavenumbers studied.

Acknowledgements

The V1D1 code was developed at the British Antarctic Survey in Cambridge, UK. Many of the original aspects of the code were developed by R. B. Horne and M. P. Freeman - they are the true architects of this code!

Chapter 3

The 1D Vlasov Code (v1d1)

The Vlasov simulation code discussed in this chapter is a new code, written in Fortran 90, which is based upon an electrons-only code written by R. B. Horne in Fortran 77 (modified by M. P. Freeman) [*Horne and Freeman,* 2001]. The new Vlasov simulation code uses the same algorithms as in the electrons-only code for integrating forward the Vlasov equation in time (the MacCormack method), for treatment of the electric field (Ampère's Law), and for calculating the velocity integrals for the moments of the distribution function (the in-pairs method). However, these algorithms were re-written in Fortran 90 to optimize the opportunities for running the code in parallel. The other new aspects of the code include the extension to two plasma species, better implementation of the periodic boundary conditions, a choice of methods for dealing with simulations of non-zero current, and a new startup program which optimizes the grid size and resolution in phase space for the distribution functions. This chapter aims to describe all the main points of the Vlasov simulation code, and explain in detail all the new features of the code.

When using simulations to model plasmas, it is very important to choose the right kind of simulation. Examples of different types of plasma simulation code include fluid models, particle models and hybrid simulations and the most appropriate code to use depends greatly on the constraints of the problem and the scientific aims of the study. The types of waves present in a plasma can vary enormously, and so the best method

to use depends very much on the spatial and temporal scales of the appropriate waves. The instabilities which form the main focus of this study have small length and time scales in comparison to magnetohydrodynamic waves. This means that a fluid approach would be unsuitable. A kinetic approach is more appropriate since kinetic models allow detailed study of the resonant interaction between the plasma particles and the waves. The simulation results which are presented in this thesis are largely obtained from a code which uses the Vlasov equation to model the evolution of the plasma:

$$\frac{\partial f_\alpha}{\partial t} + \mathbf{v}.\nabla f_\alpha + \mathbf{a}.\nabla_{\mathbf{v}} f_\alpha = 0 \tag{3.1}$$

where $f_\alpha(\mathbf{r}, \mathbf{v})$ is the distribution function of particle species α. The work contained in this thesis is concerned with a plasma which has two particle species, electrons e and protons i. This is appropriate for space plasma regions such as the solar wind near the Earth and the magnetosphere, since protons are likely to be the dominant ion species. The first section in this chapter discusses the algorithms used in the Vlasov code. A discussion on the reliability of the code is the main focus of the rest of the chapter. It is very important to check that the new two-species code behaves in the same way as the original electron code in those situations where ion dynamics are not important. As a result, the two applications discussed in this chapter have been used to "test" the code to see how well it reproduces well-known linear and non-linear plasma results regarding electron plasma behaviour. The second section in this chapter gives results obtained after using the code to study Landau damping of Langmuir oscillations and the third section gives results from a study into weak growing waves.

3.1 Description of the Vlasov Code

3.1.1 Representation of the distribution function

The key strength of kinetic codes is that they allow for the evolution of the form of the distribution function. This means that there is no constraint on the form of

distribution function which can be studied. There have been many observations of non-Maxwellian distributions in space plasmas. *Montgomery et al.,* [1970], *Scudder et al.,* [1973] and *Feldman et al.,* [1983] describe observations of flat-topped electron distribution functions downstream of the Bow Shock in the magnetosheath. Distribution functions with non-thermal high energy tails have been observed in the solar wind [*Gurnett et al.,* 1979a] and in the central plasma sheet [*Christon et al.,* 1989]. There are also many observations of distribution functions which contain beam components, e.g. in the auroral ionosphere [*Cattell et al.,* 1991, *Wahlund et al,* 1998], in the low latitude boundary layer [*Ogilvie et al.,* 1984] and in the magnetotail [*Elphic and Gary,* 1990, *Frank et al.,* 1994, *Yin et al.,* 1999]. These observations demonstrate that space plasmas often have non-Maxwellian distributions and so a fluid approach is not always suitable. In this respect, kinetic codes can offer insight into the plasma processes associated with these observations where fluid codes cannot, since a fluid code can only describe changes in the bulk moments of the distribution function, not changes in the form of the distribution function.

In the Vlasov code, the distribution functions $f_\alpha(\mathbf{r}, \mathbf{v})$ are described by arrays. The rank of each array depends on the number of dimensions in phase space needed to take account of the important physics of the problem. Each calculation involving the plasma distribution functions must be applied to every point in the array, and so keeping the array rank and dimensions down to a minimum is essential to keep runtime to an acceptable level. This is the only major drawback to using Vlasov codes, since the huge arrays required to store the distribution functions can make computation very slow. With current computer resources, it is not unreasonable to use these types of codes for simpler, one-dimensional electrostatic problems. A one-dimensional problem requires an array to describe the distribution function with a rank of two, and these kinds of problems form the basis of this study.

As computers become more efficient, the types of waves studied with these type of codes can become more and more complicated, without either having to allow for a large impractical increase in runtime, or having to make compromises in the resolution

of each dimension of the arrays. It should also be noted that kinetic particle codes also face the problem of large memory use and long runtime, since they describe the distribution functions using collections of superparticles. In order that the numerical particle diffusion due to thermal fluctuations be kept to a minimum, the numbers of these superparticles can often run to many millions [*Omura et al.,* 1996]. Further discussion of one-dimensional particle codes is given in Chapter 4.

In order to study a one-dimensional problem, the distribution function needs to be defined for two directions in phase-space, one spatial direction and one velocity direction. Without loss of generality, we define these directions as z and v_z. We define the array which describes the distribution function on a two-dimensional phase-space grid in the simulation box. Note that this box must have finite dimensions, and so boundary conditions must be imposed in each of the two directions in phase space. The boundary conditions depend very much on the physical situation under consideration and choosing the correct boundary conditions for the problem is very important. For general one-dimensional electrostatic wave studies, periodic spatial boundary conditions are the most appropriate. The box can then be imagined to represent a repeatable part of an infinite plasma, and so the results from the simulation can be applied to a larger system than the box dimensions indicate. The boundary conditions in velocity space are chosen to be a fourth-order interpolation. It is assumed that the size of the box is chosen such that the distribution functions tend to zero at the limits of the velocity grid, and so this choice of velocity boundary condition is appropriate.

The length of the box and the grid spacing need to be chosen with care. For the spatial dimension, the length of the box L_z should be at least the size of the longest wavelength which is important in the plasma simulation. If there is more than one wave mode present in the plasma, it is necessary to solve the linear dispersion relation to find the value of the longest important wavelength which is likely to be present in the linear growth phase of the instability to be studied. The solutions of the linear dispersion relation can be found numerically using a Newton-Raphson root-

finding algorithm for a range of values of wavenumber k_z (see Section 2.2.3). The grid spacing in the spatial dimension Δz is determined by two characteristic lengths: the Debye length of the plasma, and the shortest important wavelength. The grid spacing should be of the order of a Debye length, but more importantly, it should be small enough to adequately resolve the shortest wavelength which is important to the system. Again, if there is more than one wave mode present in the plasma, it is necessary to numerically solve the linear dispersion relation in order to see which wavelengths are likely to be present. The spatial grid is defined so that the indices of the points run from 0 to N_z where $N_z = L_z/\Delta z$.

When choosing the size and spacing for the velocity dimension, less obvious constraints apply. The size of the velocity dimension should be such that at the edge of the box, the value of the distribution function remains close to zero. A finite box can result unphysical increases in the values of f at the velocity boundary which occur if the plasma is accelerated towards the cut-off velocity. Keeping the velocity cut-offs v_{cut} high enough will ensure that these accumulations do not significantly alter the distribution function at lower velocities [*Chanteur,* 1984]. It is also important to make sure that the velocity cut-off for each plasma species is larger than the highest phase velocity of the unstable waves, else the resonant interactions between the waves and the particles will not take place. Appropriate velocity cut-off values can range from 5 to 20 times the thermal speed of the plasma species. The velocity cut offs are selected to ensure that the zeroth, first and second moments of the distribution functions are accurate, and to ensure that the phase velocities of the unstable waves are resolved by the velocity grid. The velocity grid is set up so that the indices of the grid points run from $-N_v$ to $+N_v$ where $N_v = v_{cut}/\Delta v_z$ is the number of points which resolve velocity space between 0 and v_{cut}. The velocity grid spacing Δv_z should be such that at the phase velocities of the waves, there is sufficient resolution that the wave particle interactions can be studied. The phase velocities which are important for the simulation are calculated from the solutions to the linear dispersion relation. We enforce this condition by ensuring that $\Delta v_z < (v_{ph,max} - v_{ph,min})$. It is also desirable

to have at least 10 grid points representing the half-width of the distribution function so that the bulk part of the distribution is adequately resolved. Note that although the spatial grid sizes of all the distribution functions should be the same, since it is through the spatial dimension that the electric field is coupled to the distribution function, there is no such constraint on the velocity grid, and so these can be tailored to the distribution function of each species.

We believe that the phase-space grid optimizing routines at the beginning of the program form a unique feature of this Vlasov simulation code. *Nunn et al.,* [1997] describe in detail the conditions which have to be met by the phase-space grid in order to simulate the VLF (very low frequency) chorus in the Earth's magnetosphere, but as far as can be determined in the available literature, this Vlasov code is the only code which includes all the criteria and conditions pertinent to electrostatic longitudinal unmagnetized instabilities in an automatic grid size and resolution finding algorithm at the beginning of each simulation run. This program should ensure a tailor-made grid for every simulation run, given the initial bulk moments (number density, drift velocity and temperature) of the plasma. If distribution functions were used to initiate the simulation which could not be expressed as a sum of drifting Maxwellian distributions, then some of these initial criteria might have to be modified. However, for all the simulation runs documented in this thesis, the grid optimization algorithms prove to be a very useful way of ensuring that all the important physics of the problem can be handled by the simulation grid, whilst keeping the sizes of the simulation arrays to a minimum.

3.1.2 Governing equations

There are two key equations in the Vlasov code. The Vlasov equation [Eq. (3.1)] is used to numerically integrate forward the distribution functions in time. In one-dimension, assuming no magnetic field in the z-direction, the Vlasov equation becomes:

$$\frac{\partial f_\alpha}{\partial t} + v_z \frac{\partial f_\alpha}{\partial z} + \frac{q_\alpha}{m_\alpha} E_z \frac{\partial f_\alpha}{\partial v_z} = 0 \tag{3.2}$$

In order to obtain the evolution of the electric field, Ampère's Law is used to integrate the electric field forward in time;

$$\frac{\partial E_z}{\partial t} = -\mu_0 c^2 J_z \tag{3.3}$$

The current density, J_z can be calculated from the sum of the first moments of the distribution functions;

$$J_z = \sum_\alpha q_\alpha \int_{-\infty}^{\infty} v_z f_\alpha dv_z \tag{3.4}$$

This gives a set of coupled equations which can be used to model how the system behaves under the influence of electrostatic waves. Many other one-dimensional electrostatic Vlasov codes rely on the Poisson equation to obtain the electric field at each time step [*Singh,* 1980, *Chanteur,* 1984, *Wang et al.,* 1997, *Schumer and Holloway,* 1998, *Califano and Lontano,* 1999, *Fijalkow,* 1999]. Since the Poisson equation involves a spatial derivative of the electric field, it is necessary to impose spatial boundary conditions on the electric field as well as on the distribution function. However, by using Ampère's Law instead, there is no need to impose explicit spatial boundary conditions on the electric field.

Constraints also need to be imposed on the time step used in the simulation. In order to ensure stability, two conditions need to be met. The first is the Courant-Friedrich-Lewy condition [*Anderson,* p.99, 1992];

$$\Delta t \leq \frac{\Delta z}{v_{cut}} \tag{3.5}$$

In order to preserve both accuracy and stability, let $v_{cut}\Delta t/\Delta z = 0.8$, where 0.8 is known as the Courant number. The other condition on the time step is that information should not propagate across more than one velocity grid cell in one time step [*Horne and Freeman,* 2001];

$$\Delta t \leq \frac{m_\alpha}{q_\alpha}\frac{\Delta v}{E_{max}} \tag{3.6}$$

Satisfying these two conditions should ensure stability of the solutions of the simulation.

The numerical algorithm used in the code for evolving the distribution function is MacCormack's method [*Anderson,* p.128-131, 1992]. This is an explicit finite-difference method which uses a predictor-corrector algorithm. It has the advantage of using first-order derivatives to calculate a second-order accurate solution. In order to evolve the electric field, a central difference method is used. It too is second-order, and tests of the simulation have shown that it gives identical results to using the MacCormack method for the electric field. The central difference method has the advantage of only involving one calculation per time step. The method is implemented as follows, remembering that equations involving the distribution function must be performed separately for each plasma species.

The first predictor step requires that the time derivative on the left hand side of the Vlasov equation (Eq. 3.1) be calculated using forward finite differences for the spatial and velocity derivatives of the known distribution function at time t in order to calculate f_α at $t = t + \Delta t$. Let the indices i, j indicate the value of f_α at each discrete point in real space and velocity space respectively, and for the moment, we will drop the subscript α which denotes plasma species. Note that a forward finite difference uses information at the $i+1$ or $j+1$ grid point to calculate the derivative, and a backward finite difference uses the information at the $i-1$ or $j-1$ grid point to calculate the derivative. The forward finite difference for $(\partial f_{i,j}/\partial t)$ is therefore:

$$\frac{\partial f_{i,j}}{\partial t} = -v_j \left(\frac{f_{(i+1),j}(t) - f_{i,j}(t)}{\Delta z} \right) - \frac{q_\alpha}{m_\alpha} E_i(t) \left(\frac{f_{i,(j+1)}(t) - f_{i,j}(t)}{\Delta v_z} \right) \tag{3.7}$$

These "next-neighbour" calculations can be efficiently performed on the whole distribution function array by using the `eoshift` intrinsic function in Fortran 90 to obtain the $f_{(i+1),j}(t)$ array. This removes the need for large nested do-loops. Now we use this time derivative to predict the distribution function at the next time step using a first-order Taylor expansion:

$$\overline{f_{i,j}(t + \Delta t)} = f_{i,j}(t) + \Delta t \frac{\partial f_{i,j}}{\partial t} \tag{3.8}$$

The predicted value of $\overline{f_{i,j}(t + \Delta t)}$ is used to give a "corrected" time derivative which is calculated using backward finite differences for the spatial and velocity derivatives

on the right hand side:

$$\left(\overline{\frac{\partial f_{i,j}}{\partial t}}\right) = -v_z\left(\frac{\overline{f_{i,j}(t+\Delta t)} - \overline{f_{(i-1),j}(t+\Delta t)}}{\Delta z}\right) - \frac{q_\alpha}{m_\alpha}\overline{E_i(t+\Delta t)}\left(\frac{\overline{f_{i,j}(t+\Delta t)} - \overline{f_{i,(j-1)}(t+\Delta t)}}{\Delta v_z}\right) \tag{3.9}$$

where $\overline{E_i(t+\Delta t)}$ is the value of the electric field at the next time step calculated by integrating forward Ampère's Law using a central difference method. The new value of $f_{i,j}(t+\Delta t)$ is then calculated using an average of the predicted time derivative and the corrected time derivative:

$$f_{i,j}(t+\Delta t) = f_{i,j} + \frac{\Delta t}{2}\left(\frac{\partial f_{i,j}}{\partial t} + \left(\overline{\frac{\partial f_{i,j}}{\partial t}}\right)\right) \tag{3.10}$$

Thus by using only first-order derivatives, a second-order accurate solution can be obtained. Tests of the code showed that accuracy is improved if this algorithm is applied in a "flip-flop" fashion: if the time step is even, then the predictor step is calculated using forward finite differences for the spatial and velocity derivatives and the corrector step using backward finite differences; if the time step is odd, then backward finite differences are used for the predictor step and forward finite differences for the corrector step.

At each time step, the first three moments of the distribution function are calculated in order to obtain the bulk plasma properties (see Chapter 2). The algorithm used to calculate these moments [for the plasma parameters as well as the current in Eq. (3.4)] is known as an in-pairs integration method [*Horne and Freeman,* 2001]. Using the number density calculation as an example, the integral can be calculated numerically as follows:

$$n_\alpha(z,t) = \int_{-\infty}^{\infty} f_\alpha(z,v_z,t)dv_z = \sum_{i=-N_v}^{N_v-1}\frac{1}{2}\left[f_\alpha(z,i,t) + f_\alpha(z,i+1,t)\right]\Delta v_z \tag{3.11}$$

To improve accuracy, the terms of the sum are added in pairs around $i = 0$ so that terms of the same order are added together:

$$n_\alpha(z,t) = \left[\frac{1}{2}f_\alpha(z,-N_v,t) + \frac{1}{2}f_\alpha(z,N_v,t) + \sum_{i=-N_v}^{0}\left[f_\alpha(z,i,t) + f_\alpha(z,-i,t)\right]\right]\Delta v_z \tag{3.12}$$

This ensures that almost all of the smallest terms in the sum are added first, which improves accuracy. In tests against two other methods, the in-pairs method proved to be the most accurate [*Horne and Freeman,* 2001] even for a coarse velocity grid resolution.

3.1.3 Imposing spatial boundary conditions

As discussed in Section 3.1.1, the spatial boundary conditions for the Vlasov code are periodic. These are relatively easy boundary conditions to implement, since all that is required is that $f_\alpha(0, v_z, t) = f_\alpha(N_z, v_z, t)$ and $f'_\alpha(0, v_z, t) = f'_\alpha(N_z, v_z, t)$. The continuity of the spatial derivative is achieved in the code by assigning values of the distribution function to a spatial grid with indices $(-1 : N_z + 1)$ where $f_\alpha(-1, v_z, t) = f_\alpha(N_z - 1, v_z, t)$ and $f_\alpha(N_z + 1, v_z, t) = f_\alpha(1, v_z, t)$. This ensures that when the `eoshift` function is applied, the derivatives are calculated for all $f_\alpha(0 : N_z, v_z, t)$ without special consideration needed for the boundary values. After each successive time integration using the MacCormack method, the end points are assigned to their appropriate counterparts. Repeated checks on the electric field at the spatial boundaries have shown that this method also ensures that the periodic boundary conditions are observed by the electric field, without the need for explicit enforcement.

3.1.4 Filamentation

One of the key limitations of Vlasov codes is the problem of filamentation. As waves damp or grow in the simulation, fine structure will develop in the distribution function. This is a physical effect, and is expected from solutions to the Vlasov equation (see, for example, *Krall and Trivelpiece,* Section 8.7, [1977]). However, this fine structure can cause large velocity derivatives to develop because of the discrete nature of the velocity grid. Once the fine structure becomes comparable to the velocity grid spacing, unphysical numerical diffusion will occur due to the large velocity derivatives, and this can cause the simulation to fail. Although there are numerical methods which can

solve this problem by performing the simulation calculations with filtered distribution functions [*Klimas,* 1987], these methods result in a loss of resolution of the distribution function (note that the solutions are unaffected by the filtering, but the distribution function output from the code can only have limited resolution in velocity space). The problem of filamentation only becomes important after long times have passed in the simulation. The results to be presented in this thesis are taken from periods before this fine structure has had a chance to develop. The velocity grids are also chosen so that they have sufficient resolution that the required results from the simulations can be obtained before this problem leads to unphysical results.

A numerical problem which is related to filamentation, but which is entirely unphysical, is that of recurrence. The recurrence effect results from imposing periodic boundary conditions and having regularly spaced velocity grids. Although the Vlasov simulation deals with distribution functions and not individual particles, it is more straightforward to explain this effect in terms of particle behaviour. After a time $T_r = 2\pi/k\Delta v$, the particles in the lowest velocity grid cell will have traveled one wavelength, and will have returned to the same phase on the wave with wavenumber k. In this time, the particles on other velocity grid cells at integer multiples of Δv will have traveled integer multiples of a wavelength and will also have returned to the same phase. Hence, in the absence of particle trapping effects, the distribution function will be reconstituted at $t = T_r$ [*Horne and Freeman,* 2001]. Most of the simulation results reported in this thesis deal with growing waves, so there is likely to be sufficient particle trapping that the recurrence effect will not affect the results, but the Landau damping results discussed in Section 3.2 will only be valid for $t < T_r$.

3.1.5 Simulating a plasma with a finite current in one dimension

In order to simulate current-driven ion-acoustic waves, it is necessary to consider a plasma with a finite current. If a finite current is present in one-dimension, then consideration must be given when implementing Ampère's Law to integrate the electric

field forward in time. It is necessary to return to the full Ampère's equation in three dimensions and consider the influence of a net current on the magnetic field.

Since our spatial boundary conditions are periodic, we assume a uniform current in the z-direction. The uniform current will induce a magnetic field which varies only in the perpendicular directions to z, if the current is uniform along z. Consider the Maxwell-Ampère equation in the z-direction only;

$$\frac{\partial B_x}{\partial y} - \frac{\partial B_y}{\partial x} = \mu_0 J_z + \frac{1}{c^2}\frac{\partial E_z}{\partial t} \tag{3.13}$$

Take the Fourier transform of this equation with respect to z;

$$\frac{\partial \tilde{B}_x(k)}{\partial y} - \frac{\partial \tilde{B}_y(k)}{\partial x} = \mu_0 \tilde{J}(k) + \frac{1}{c^2}\frac{\partial \tilde{E}(k)}{\partial t} \tag{3.14}$$

where $\tilde{B}_x(k)$ is the Fourier transform of $B_x(z)$. The above equation holds separately for each value of k, thus it can be used here to form two equations, one where $k = 0$ and one where $k \neq 0$;

$$\frac{\partial \tilde{B}_x(0)}{\partial y} - \frac{\partial \tilde{B}_y(0)}{\partial x} = \mu_0 \tilde{J}(0) + \frac{1}{c^2}\frac{\partial \tilde{E}(0)}{\partial t} \tag{3.15}$$

$$0 = \mu_0 \tilde{J}(k \neq 0) + \frac{1}{c^2}\frac{\partial \tilde{E}(k \neq 0)}{\partial t} \tag{3.16}$$

The left hand side of Eq. (3.16) is set to zero because it is assumed that the simulations will excite electrostatic waves, and so the magnetic field associated with $(\partial E(k \neq 0)/\partial t)$ is negligible, and can therefore be neglected. Taking inverse Fourier transforms of these two equations gives;

$$\frac{\partial B_{0x}}{\partial y} - \frac{\partial B_{0y}}{\partial x} = \mu_0 J_0 + \frac{1}{c^2}\frac{\partial E_0}{\partial t} \tag{3.17}$$

where a zero subscript denotes a spatially-averaged quantity, and;

$$\mu_0 J_1(z) + \frac{1}{c^2}\frac{\partial}{\partial t} E_1(z) = 0 \tag{3.18}$$

where $J_1 = J - J_0$ and $E_1 = E - E_0$ are the perturbed quantities.

So by using this separation of the spatially-averaged and oscillating part, it is possible to model a plasma environment with non-zero current in one dimension. It

can be said that Eq. (3.17) describes the macroscopic character of the system, and Eq. (3.18) the wave-particle interactions in the system.

There are two ways to treat Eq. (3.17) in the simulation code without explicitly calculating the magnetic field: one is to assume that the left hand side always balances the current in the system, and so there is no displacement current at all, and the other is to assume the system is magnetostatic, i.e. the left hand side of the equation stays constant throughout the simulation. For most of the simulation results in Chapters 4 and 5, the first case is used, and there is assumed to be no displacement current present in the system. These assumptions are similar to those used by *Omura et al.,* [1996] when simulating beam-driven electrostatic instabilities in the magnetotail. There is also a comparison in Chapter 4 between two runs each using a different treatment of Eq. (3.17).

3.2 Landau damping of electrostatic Langmuir oscillations

The first test of the Vlasov code was to see whether it could reproduce Landau damping of Langmuir oscillations in a field-free plasma. Landau damping is a thermal effect whereby electrostatic waves dissipate their energy in a warm collisionless plasma by exchanging energy with the particles. This effect is predicted by kinetic theory, and a comprehensive analytical treatment can be found in all standard textbooks [e.g. *Krall and Trivelpiece,* Ch. 8, 1973, *Swanson,* Ch. 4, 1989, *Stix,* Ch. 16, 1992]. From Chapter 2, the linear dispersion relation for high-frequency electrostatic waves in one-dimension for a thermal field-free plasma is:

$$D(\mathbf{k},\omega) = 1 - \frac{\omega_{pe}^2}{v_{te}^2 k^2} Z'\left(\frac{\omega}{k v_{te}}\right) = 0 \tag{3.19}$$

assuming that the electron distribution function is Maxwellian and that the ion contribution can be ignored because we are concentrating on high frequency oscillations $\omega_r \sim \omega_{pe}$. Numerical solutions of this linear dispersion relation are given in Figure 3.1 for an electron temperature $T_e = 0.1$ eV and number density $n_e = 9 \times 10^5$

m^{-3}. These are the parameters which are to be used for each of the two Landau damping simulation runs described below.

The solutions of the dispersion relation show that above $k \sim 0.2\lambda_{De}^{-1}$, there is damping of the Langmuir waves (i.e. $\gamma < 0$). We will study both strong and weak Landau damping of a Langmuir oscillation and so two wavenumbers were chosen, $k = 0.27\lambda_{De}^{-1}$ which is weakly damped and shown with triangles in Figure 3.1, and $k = 0.54\lambda_{De}^{-1}$ which is strongly damped and shown by the squares. A separate simulation run is performed for each of these waves. In each case, only one wavenumber is present in the simulation, and it's evolution is studied. These simulation runs are not intended to reflect a real physical situation, but are performed in order to check that the Vlasov simulation code can reproduce well-known analytical results. In order to model the response of the plasma to each of these oscillations, the size of the simulation box is set in each case to equal the wavelength of the oscillation, and a standing wave of the form:

$$E(z,t) = E_0(\sin(kx - \omega t) + \sin(kx + \omega t)) \tag{3.20}$$

is applied across the simulation box at $t = 0$. The perturbations in electron number density and drift velocity are calculated at $t = 0$ using the Poisson equation and Ampère's Law respectively, and these perturbations are used to modify the initial electron distribution function, which is Maxwellian:

$$f_e(z, v_z, t) = \frac{n_e}{v_{te}\pi^{1/2}} \exp\left(-\frac{v^2}{v_{te}^2}\right) \tag{3.21}$$

In each of the following cases, the initial electric field amplitude $E_0 = 0.5$ mVm^{-1}. A number of runs were made for the same initial conditions, but with different initial electric field amplitudes ranging from $E_0 = 0.5$ pVm^{-1} to $E_0 = 0.5$ Vm^{-1}. No qualitative differences in the results were seen, so the choice of initial electric field amplitude does not influence the qualitative behaviour of the plasma in response to the electric field. Note, however that the amplitude of electrostatic noise due to thermal fluctuations in a plasma can be given by [*Treumann and Baumjohann,* p.25,

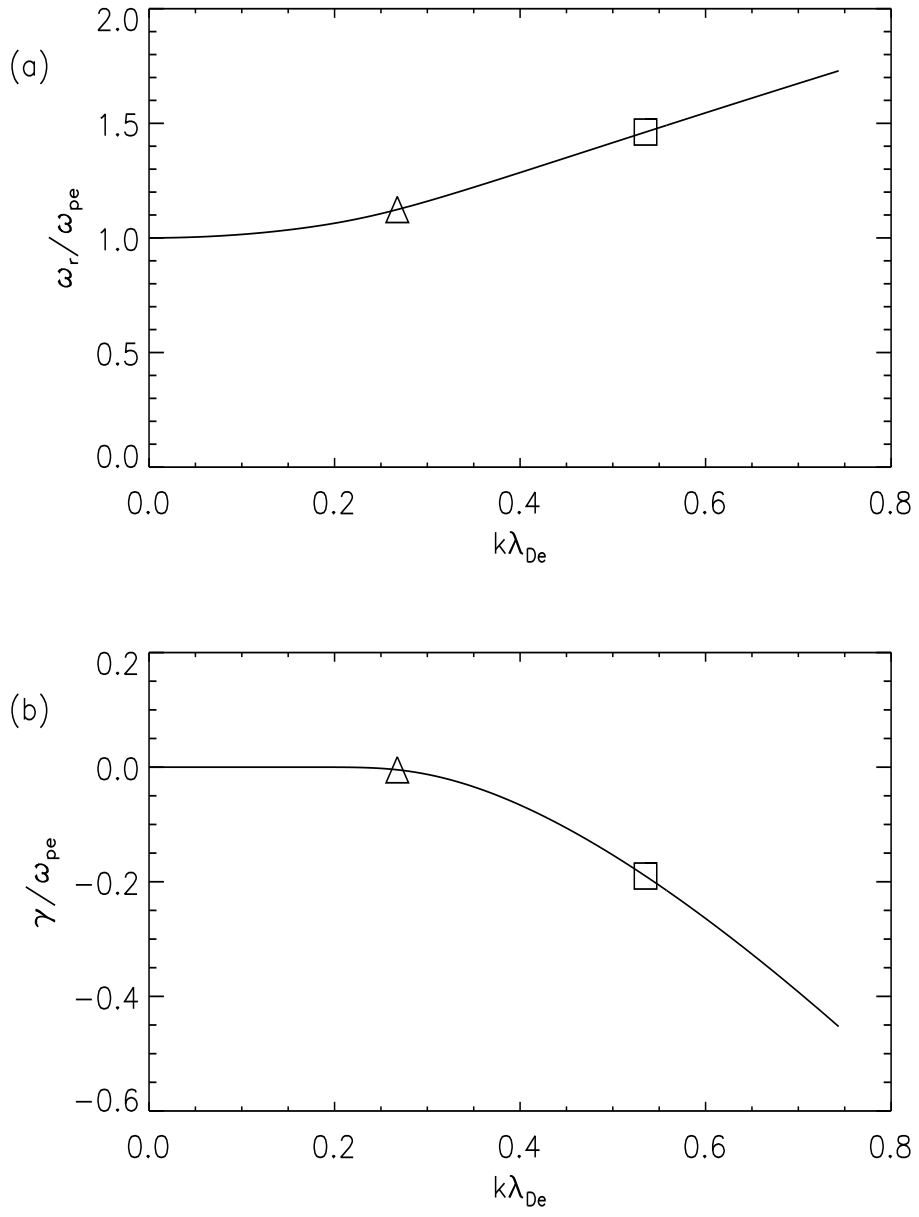

Figure 3.1: *Numerical solution of the electrostatic dispersion relation showing (a) real part and (b) imaginary parts of frequency for each wavenumber k ($T_e = 0.1$ eV, $n_e = 9 \times 10^6$ m^{-3}). Triangles indicate wavenumber chosen as an example of weak damping and the squares show the wavenumber chosen to represent strong damping.*

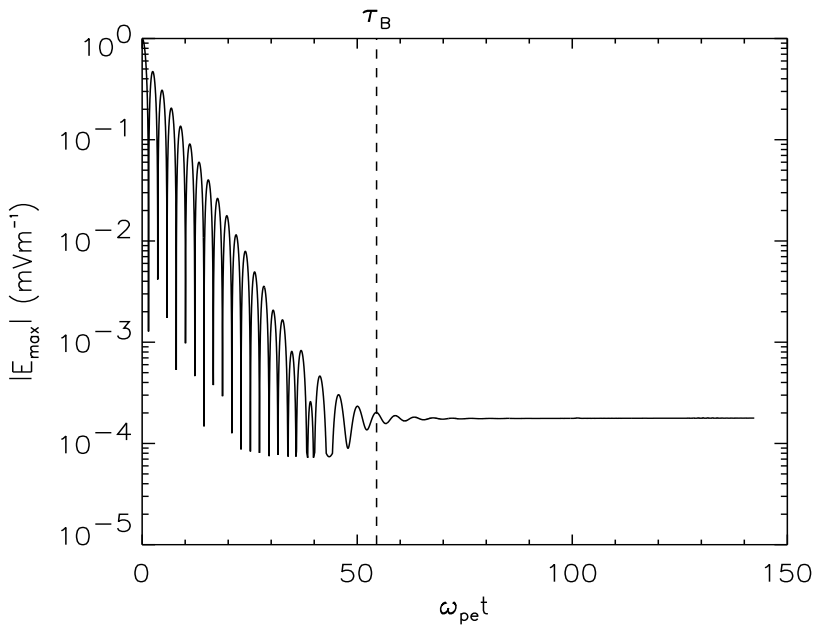

Figure 3.2: *Evolution of the maximum electric field amplitude for standing wave with* $k = 0.54\lambda_{De}^{-1}$. *The dotted line shows* $t = \tau_B$, *where* τ_B *is the bounce time of the electrons for the wave initially applied to the simulation box.*

1997]:

$$E_{tf} = \left(\frac{2k_B T_e}{\epsilon_0 \lambda_{De}^3}\right)^{1/2} \tag{3.22}$$

For these initial parameters, $E_{tf} = 15.0\ \mu\mathrm{Vm}^{-1}$ and so any results from these simulation runs concerning electric field amplitudes less than this value have little physical relevance, since the damping would not be observed in a real plasma. However, the runs which start with a very low electric field amplitude show how little numerical noise is present in a Vlasov code. This is one of the reasons that Vlasov codes are well suited for studying microphysical processes in plasmas in great detail. The low numerical noise of the Vlasov simulation also avoids the need to use extreme initial conditions in order to excite unstable waves. If there is a lot of noise in the system, then it is necessary to excite very strong unstable waves which will grow above the noise level in a short time. The Vlasov simulation code can be successfully used to study the evolution of both strong and weak instabilities.

Consider first the oscillation with $k = 0.54\lambda_{De}^{-1}$. The damping rate of this wave,

which is given by the imaginary part of the solution to the linear dispersion relation, is $\gamma = -0.19\omega_{pe}$. This wave can be said to be strongly Landau damped, since γ is relatively large compared to the real part of the frequency ($\omega_r = 1.1\omega_{pe}$). Figure 3.2 shows the evolution of the maximum electric field $E_{\max}$ in the box for $t < \tau_B$ where τ_B is the bounce time of the plasma [*Swanson,* p.140, 1989];

$$\tau_B = \sqrt{\frac{m_e}{|q_e|E_0 k}} \tag{3.23}$$

The bounce time is the reciprocal of the frequency at which trapped particles will oscillate in the potential well of the electric field oscillation. Particle trapping is a non-linear phenomenon and so to study linear Landau damping, it is necessary to consider times less than the bounce time, which in this case is $\tau_B = 54.5\omega_{pe}^{-1}$. The growth rate calculated from performing a linear regression fit to the peaks in Figure 3.2 for the time period $5\omega_{pe}^{-1} \leq t \leq 25\omega_{pe}$ is $\gamma_{\text{meas}} = -0.199 \pm 0.003\omega_{pe}$. This compares favorably with $\gamma = -0.19\omega_{pe}$ calculated using the linear dispersion relation. The error gives the 95% confidence level in the linear regression fit. We can be confident that the code performs well for strong Landau damping in the linear regime $t < \tau_B$.

The recurrence time for the above simulation run $T_r = 498\omega_{pe}^{-1} \gg \tau_B$ is long after the electric field amplitude has leveled out. This means that recurrence effects should not be important in the evolution of the damped wave as observed in this simulation run.

This simulation was run for times longer than the bounce time. After τ_B, $E_{\max}$ does not decay, and stays at a steady value of $\sim 0.2\ \mu\text{Vm}^{-1}$. This is believed to be due to the method of initializing the standing wave. The wave described by Eq. (3.20) is a time-asymptotic solution of the field-free Vlasov equation. This late-time solution does not account for the ballistic, or free-streaming contribution to the perturbation, which does not decay. For more than the simplest of initial conditions, it is impossible to know the exact form of this ballistic contribution [*Krall and Trivelpiece,* p.392-5, 1973] and so this leads to a numerical error in the code which manifests itself as a perturbation of constant amplitude which dominates once the Langmuir oscillation has damped to below a certain amplitude. As mentioned above, many simulation

runs were performed for different initial oscillation amplitudes. In each case, the wave amplitude decayed by the same number of orders of magnitude, before leveling out. Note that for this particular case, however, this final level is less than the value of the field due to thermal fluctuations, and so for simulation runs with initial E_0 less than three orders of magnitude above the thermal fluctuation level, this problem is not important. Note that the electric field noise due to thermal fluctuations is not present in the Vlasov code unless it is explicitly added. The initial distribution functions are smooth functions, and do not exhibit the thermal fluctuations which would be present in a particle code, and in the real plasma. For all of the Landau damping runs, the electric field due to thermal fluctuations is absent from the simulation. However, in order to excite growing waves, the electric field noise due to thermal particle motions is added at $t = 0$.

The second Landau damping run studies the evolution of a standing wave with wavenumber $k = 0.27\lambda_{De}^{-1}$. In this case the corresponding damping rate is much weaker, $\gamma = -5 \times 10^{-3}\omega_{pe}$. Figure 3.3(a) shows $E_{\max}$ during this simulation run. Since this Langmuir oscillation is weakly damped, non-linear particle trapping effects become more significant than in the strongly damped case, and can affect the oscillation amplitude when it is still quite high. Figure 3.3(a) shows that the oscillation is not monotonically damped, but enjoys periods of growth as well. This phenomenon can be dealt with analytically [*O'Neil,* 1965] by extending the Vlasov solutions to times longer than τ_B and considering the response of the resonant electrons (those with velocities close to the phase velocity of the Langmuir wave). The oscillations in amplitude of the Langmuir standing wave are due to resonant electrons trapped in the potential well of the electric field. Experimental observations have also confirmed this effect [*Wharton et al.,* 1968]. For this simulation run, $\tau_B = 77.2\omega_{pe}^{-1}$. The first minimum in the electric field amplitude occurs at roughly $80\omega_{pe}^{-1}$, so this is consistent with the idea that the oscillations in amplitude are due to particle trapping. Note that the period of the oscillation in $E_{\max}$ appears to lengthen as the simulation progresses. This is because after each decay/growth cycle, the maximum electric field

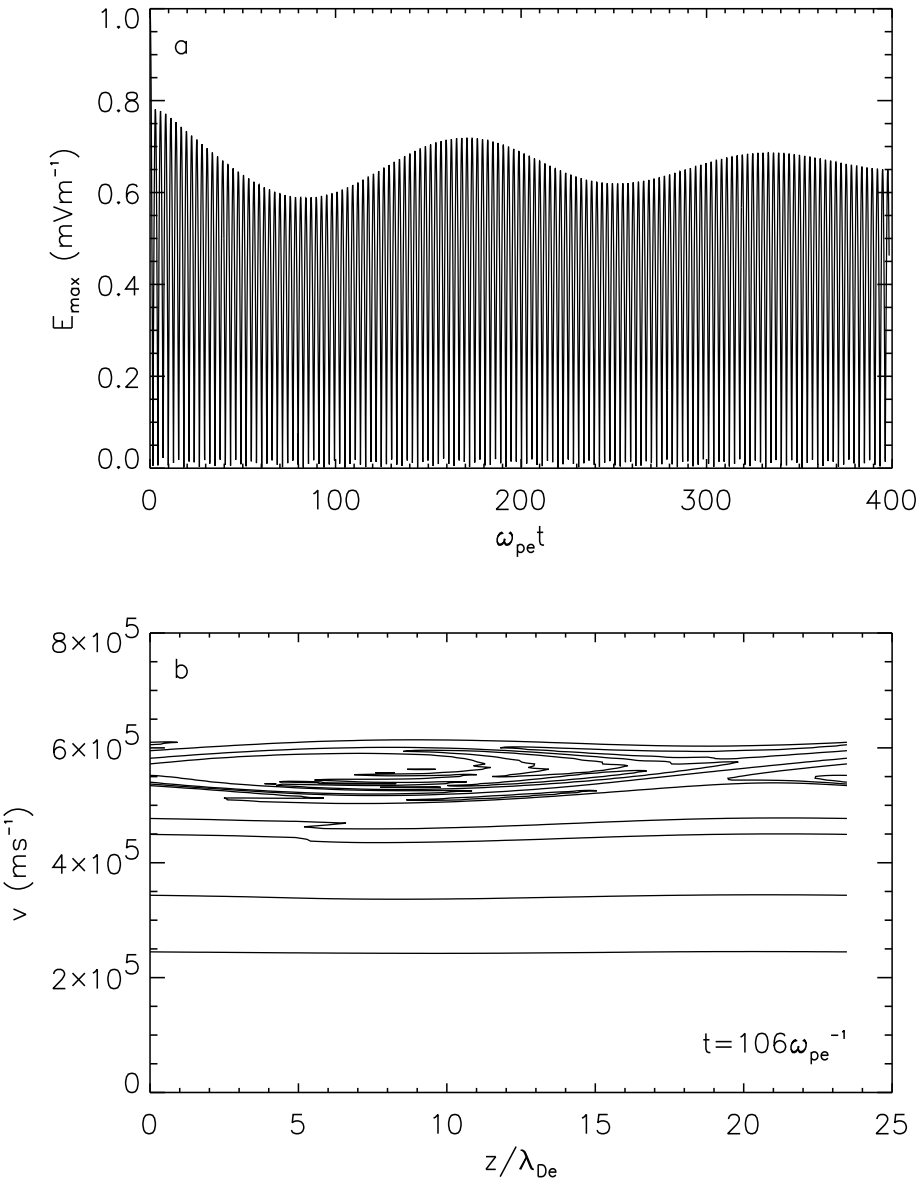

Figure 3.3: *(a)Evolution of the electric field amplitude for a standing Langmuir oscillation experiencing non-linear Landau damping; (b) contour map of the electron distribution function at* $t = 106\omega_{pe}^{-1}$ *which shows clear electron trapping at the phase velocity of the wave* $v_{ph} = 5.57 \times 10^5\ ms^{-1}$*. Contours are spaced logarithmically, showing orders of magnitude (0.1,0.01,0.001, etc) and half these values (0.05,0.005, etc).*

amplitude becomes smaller, and so the bounce time for the next period of decay is lengthened slightly [see Eq. (3.23)]. Again, the recurrence time for this simulation run $T_r = 996\omega_{pe}^{-1} \gg \tau_B$, and so recurrence effects are not important for the period of evolution studied here.

Figure 3.3(b) shows the electron distribution function f_e for a portion of phase space (all z and $v_z > 0$). The contours are spaced to show the particle trapping clearly, but are essentially logarithmic, leading from the maximum of f_e at $v_z = 0$ to the very small values of f_e at the top of the plot. This snapshot of f_e is taken at $t = 106\omega_{pe}^{-1}$, just after the first minimum in electric field amplitude, when the Langmuir oscillation is experiencing growth. The structure seen in f_e for velocities close to the phase velocity of the wave $v_{ph} = 5.57 \times 10^5$ ms^{-1} $\sim 3v_{te}$ indicates the particle trapping in f_e as predicted by *O'Neil,* [1965].

These results above show that the Vlasov code can successfully reproduce both linear and non-linear behaviour associated with Landau damping of Langmuir waves.

3.3 Gentle bump instability

The previous section discussed oscillations which were damped. The next case to consider with the Vlasov code is that of growing waves. Electrostatic waves do not only lose energy to particles, as in the Landau damping case, but they can also gain energy if there is a source of free energy in the plasma. If we consider again a warm plasma, this source of free energy can be provided by an electron beam drifting through a Maxwellian background population of electrons [*Krall and Trivelpiece,* p.458-462, 1973]. For this study, the electron beam exciting the growing waves will not have so large a drift velocity as to excite a fluid, streaming-type instability, but will instead have a drift velocity such that the electron distribution function appears to have a bump in the tail (hence "gentle bump" instability). The plasma parameters chosen for this simulation are therefore $T_e = 2$ eV and $n_e = 10^6$ m^{-3} for the stationary bulk distribution and $T_b = 1$ eV, $n_b = 10^5$ m^{-1} and $v_b = 2.5 \times 10^6$ ms^{-3} for the beam. Figure 3.4 shows the resulting one-dimensional distribution function for $v_z > 0$ given

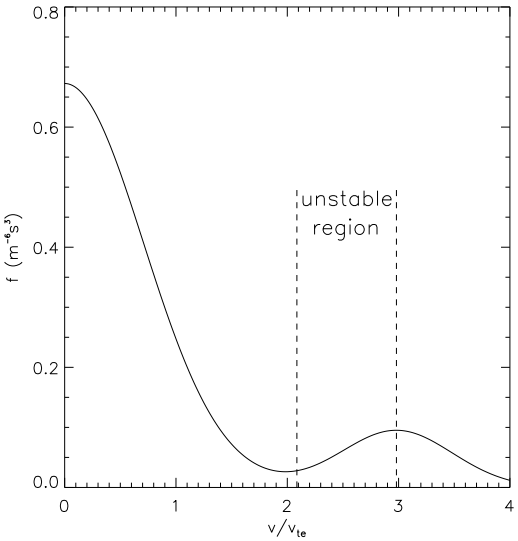

Figure 3.4: *Spatially-averaged electron distribution function showing a gentle-bump feature. The unstable region is where there is a positive gradient and is indicated by the dashed lines.*

by the following sum of Maxwellian functions:

$$\begin{aligned} f_{e0}(v_z) &= \frac{n_e}{\pi^{1/2} v_{te}} \exp\left(-\frac{v_z^2}{v_{te}^2}\right) + \frac{n_b}{\pi^{1/2} v_{te}} \exp\left(-\frac{(v_z - v_b)^2}{v_{tb}^2}\right) \\ &\quad + \frac{n_b}{\pi^{1/2} v_{te}} \exp\left(-\frac{(v_z + v_b)^2}{v_{tb}^2}\right) \end{aligned} \tag{3.24}$$

where b denotes beam quantities. The distribution function is symmetrical about $v_z = 0$ to ensure that there is no finite current in the simulation box. The region between the dashed lines is the unstable region of the distribution function. The positive gradient (negative gradient for $v_z < 0$) in this region provides the free energy needed for the waves to grow.

The one-dimensional linear dispersion relation corresponding to this distribution function is:

$$\begin{aligned} D(k,\omega) &= 1 - \frac{\omega_{pe}^2}{v_{te}^2 k^2}\left(\frac{n_e}{n}\right) Z'\left(\frac{\omega}{k v_{te}}\right) - \frac{\omega_{pe}^2}{v_{te}^2 k^2}\left(\frac{n_b}{n}\right) Z'\left(\frac{\omega - v_b k}{k v_{te}}\right) \\ &\quad - \frac{\omega_{pe}^2}{v_{te}^2 k^2}\left(\frac{n_b}{n}\right) Z'\left(\frac{\omega + v_b k}{k v_{te}}\right) \end{aligned} \tag{3.25}$$

where $n = n_e + n_b$ is the total electron number density, and the plasma frequency is calculated using n. The solutions $\omega = \omega_r + i\gamma$ of this dispersion relation for positive

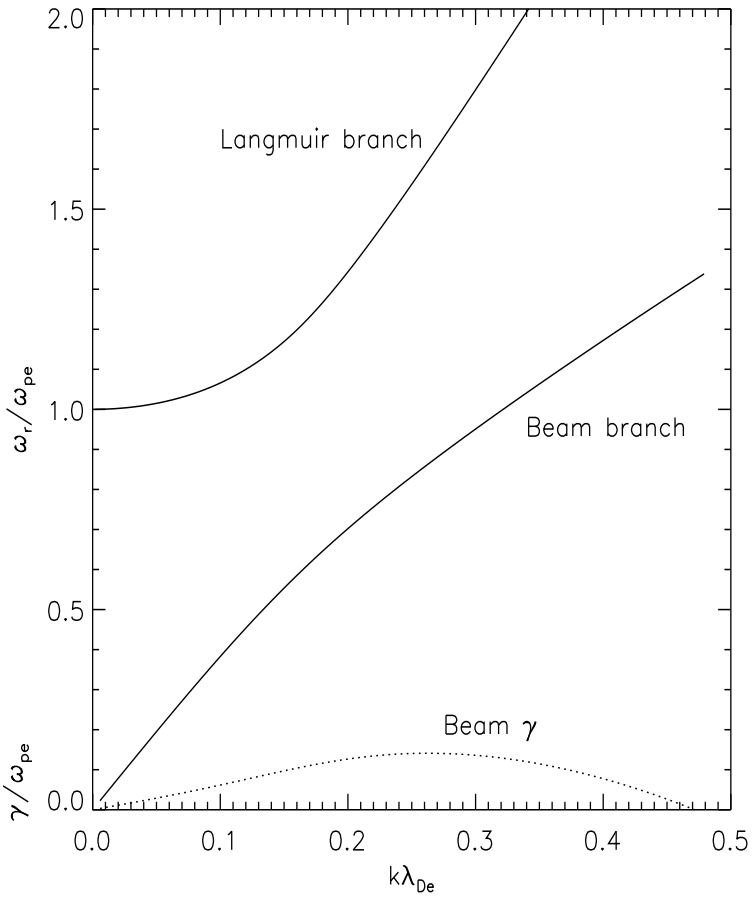

Figure 3.5: *Numerical solutions of the dispersion relation for the gentle-bump instability. There are two real frequency branches, the damped Langmuir branch and the growing beam branch. The growth rates for the beam branch are indicated by the dotted line.*

k are given in Figure 3.5. The negative k solutions are simply the positive solutions reflected in the $k = 0$ axis, and correspond to the unstable waves propagating in the $-z$ direction. All the results will be discussed in terms of the positive direction waves ($v_b > 0$) but are equally valid for the negative direction waves which are also seen in the simulation. There are two high-frequency branches of solution for this distribution function [*Gary,* 38-44, 1993], shown by the solid lines in Figure 3.5. The Langmuir branch, $\omega_r \geq \omega_{pe}$, is highly damped, the imaginary part of this solution is not shown. It is the beam mode $\omega_r \simeq kv_b$ which is the growing mode, with growth rates indicated by the dotted line.

One of the previously discussed merits of Vlasov codes is that they exhibit very little noise. As a result, in order to encourage growth of waves in the simulation, it is not simply a case of providing conditions for instability. It is also necessary to provide small perturbations in the electric field. In all the simulations dealing with growing waves, the initial perturbations in the electric field are sine waves with amplitude of the thermal fluctuations in the plasma E_{tf} with random phases:

$$E(z,0) = \sum_{m=1}^{M} E_{tf} \sin(k_m z + \phi) \tag{3.26}$$

where ϕ is the random phase and M is the maximum wavenumber of the perturbations. M can be any number between 1 (smallest wavenumber allowed which corresponds to the wave with $\lambda = L_z$) and the number of wavenumbers allowed in the simulation spatial grid (the largest wavenumber corresponds to the smallest wavelength which can be resolved by the grid). The choice of grid resolution (see Section 3.1.1) ensures that there are a number of spatial grid points which resolve the smallest unstable wavelength. Hence there will be higher wavenumbers allowed in the simulation box which do not grow due to the linear instability. However, putting power into these higher wavenumbers at the initial time step can result in numerical aliasing [*Hockney and Eastwood,* p.152-160, 1988]. Numerical aliasing is an artificial effect which is caused by non-physical mode coupling to waves whose wavenumbers (frequencies) are larger (higher) than those which can be measured with the spatial (temporal) grid. These waves can still contribute to the amplitudes of waves measured at the

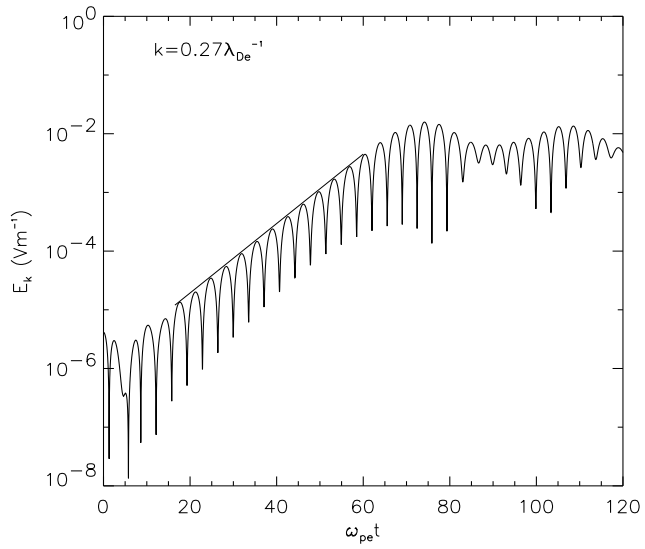

Figure 3.6: *Evolution of one of the growing modes in the gentle-bump instability run. The mode grows exponentially until* $t = 70\omega_{pe}^{-1}$*. The straight line indicates the linear fit performed on the peaks of* E_k *in order to calculate the growth rate.*

grid points and can artificially lessen or increase the amplitude, introducing numerical error into the simulation. Aliasing can sometimes manifest itself as a numerical instability which grows quickly and masks the behaviour of the physical instability. It is impossible to completely eradicate the effects of numerical aliasing, because of the finite nature of the grids used in the simulation. However, the effects of aliasing early on in the simulation can be minimized by applying electric field perturbations only to smaller wavenumbers, so that the electric field is oversampled by the spatial grid at early times in the simulation.

The electron number density is modified to be consistent with the electric field perturbations at $t = 0$ using Poisson's equation:

$$n_e(z,0) = n_e + \frac{1}{q_e}\epsilon_0 \sum_{m=1}^{M} k_m E_{tf} \cos(k_m z + \phi) \tag{3.27}$$

In order to see how well the code reproduces the linear stage of the instability, we can study the individual wave modes obtained from the electric field data. Figure 3.6 shows one of the growing modes in the simulation $k = 0.27\lambda_{De}^{-1}$. Concentrating only on the peaks of each oscillation in amplitude, the mode can be seen to grow

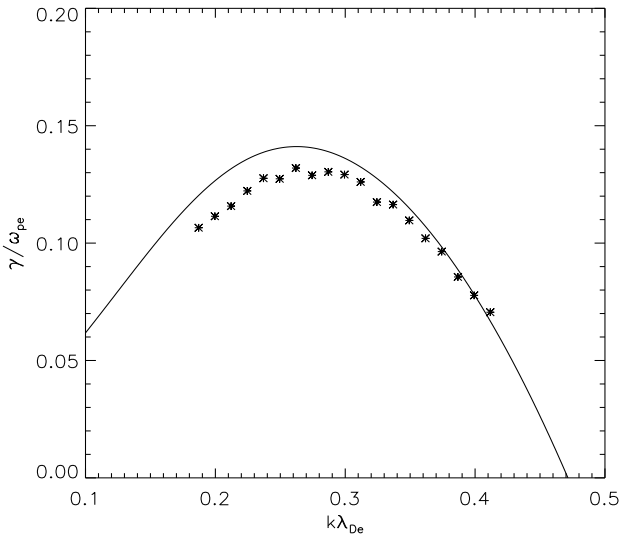

Figure 3.7: *Growth rates for the gentle-bump instability. Solid line indicates the numerical solutions of the linear dispersion relation and the stars show the growth rates calculated from the simulation results.*

exponentially from around $t = 7\omega_{pe}^{-1}$ to $t = 75\omega_{pe}^{-1}$, when it flattens out. The growth rate is calculated using a linear regression fit to the peaks of the wave mode amplitude (indicated in the plot by a straight line).

The growth rates for those modes identified as growing exponentially during early times in the simulation were calculated using this method, and plotted against wavenumber in Figure 3.7. The agreement is fairly good, although it is better for higher k. We can therefore be confident that the simulation can reproduce the linear stage of the instability fairly well.

As mentioned above, these particular wave modes do not grow exponentially for ever. At a certain time, they flatten out. This is known as saturation, and occurs because the form of the distribution function has changed in the unstable region indicated in Figure 3.4. In order for the waves to grow, they must take energy from the particles. This is known as particle scattering, since after interacting with the waves, the particles change velocity and/or direction. If enough particles change velocity, then significant changes start to appear in the distribution function. The part of the distribution function which is most likely to experience change is in the region

of resonant phase velocities. These wave-particle interactions result in the plasma acting to quench the instability by removing the conditions necessary for growth, in this case, the positive gradient of the distribution function. This plasma response can be described using quasilinear theory [*Krall and Trivelpiece,* Ch. 10, 1973, *Swanson,* Ch. 7, 1989]. A discussion of quasilinear theory as applied to changes in the bulk moments of the distribution functions can be found in Chapter 2. For the purposes of the gentle bump analysis, resonant particle diffusion leads to plateau formation over the range of resonant phase velocities so that the initially positive gradient of the beam distribution is eroded. Figure 3.8(a) shows the spatially-averaged electron distribution function for different times in the simulation. These times are indicated on a plot of the wave energy density $W_E = \frac{1}{2}\int \epsilon_0 |E_k|^2 dk$ in Figure 3.8(b) to illustrate when in the evolution of the instability these times occur. Ignoring the oscillations, the wave energy density levels out at $t = 75\omega_{pe}^{-1}$. The distribution function has formed a plateau at this time. After $t \sim 50\omega_{pe}^{-1}$ the gradient over the range of resonant phase velocities is steadily decreased as the wave-particle interactions have acted to "fill in" the distribution function.

These well-known linear and non-linear results have been successfully reproduced by the simulation, and so we can be confident that the code will also give reliable results when we turn to more complicated instabilities, such as current-driven ion-acoustic waves, which are the focus of this thesis.

3.4 Checks and Accuracy

When analyzing the results of computer simulations, it is important to consider how accurate they are. All simulation codes suffer from numerical errors to varying degrees, so it is necessary to devise checks so that the effects of these errors can be taken into account. An important measure of how well a code performs is how well it conserves macroscopic properties. The Vlasov code has periodic boundary conditions and there are no plasma sinks or sources in the system, and so it is expected that the code will conserve the integral of the distribution function over phase space, the

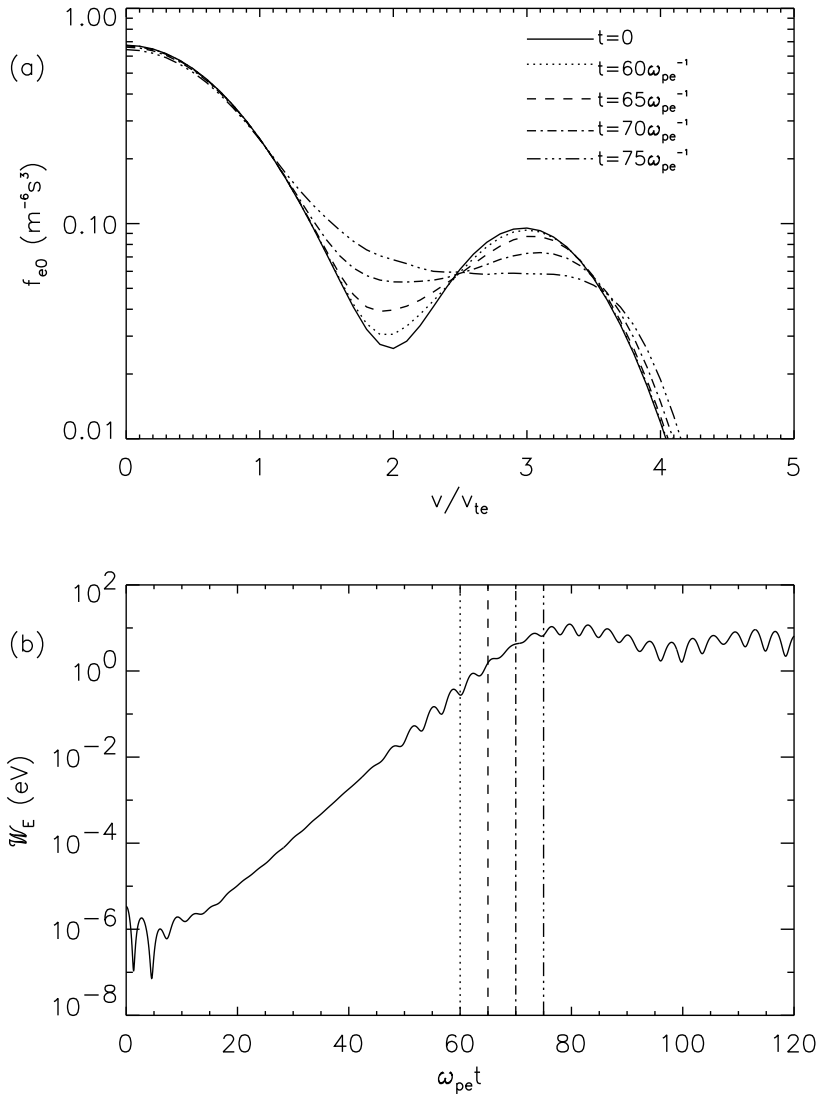

Figure 3.8: *(a) Spatially-averaged electron distribution function for different times during the simulation. The solid line indicates the initial form of the distribution function; (b) evolution of the wave energy density indicating the different times used in (a).*

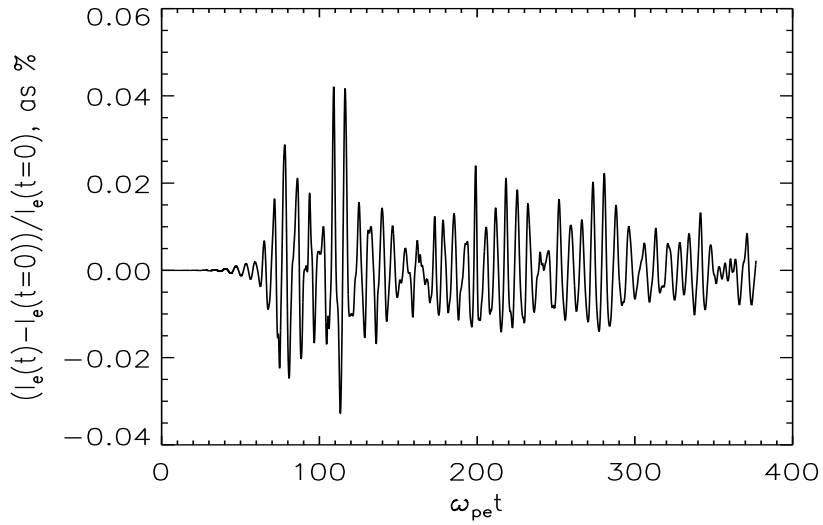

Figure 3.9: *Percentage change in the integral of the electron distribution function over phase space during the gentle-bump simulation run.*

total system energy and the total system momentum.

Let I_e be the integral of the electron distribution over phase space:

$$I_e(t) = \int f_e(z, v_z, t) dv_z dz \tag{3.28}$$

Figure 3.9 shows the percentage change in I_e throughout the gentle bump instability run discussed in the previous section (Note that Figure 3.9 shows the evolution of I_e until the simulation was ended at $\sim 380\omega_{pe}^{-1}$). This percentage change is given by:

$$\text{Percentage change in } I_e = \frac{I_e(t) - I_e(t=0)}{I_e(t=0)} \times 100 \tag{3.29}$$

There appears to be no overall change in the value of I_e throughout the simulation, although the percentage change in I_e does oscillate about zero after $\sim 35\omega_{pe}^{-1}$. The largest percentage change in I_e is 0.042%, which means that the code conserves the integral of the distribution function over phase space satisfactorily.

Next let us consider the total energy in the system. The total energy density in the simulation is a sum of the particle energy density and the wave energy density. The wave energy density is given by:

$$W_E(t) = \frac{1}{2}\epsilon_0 \int |E_k(t)|^2 dk \tag{3.30}$$

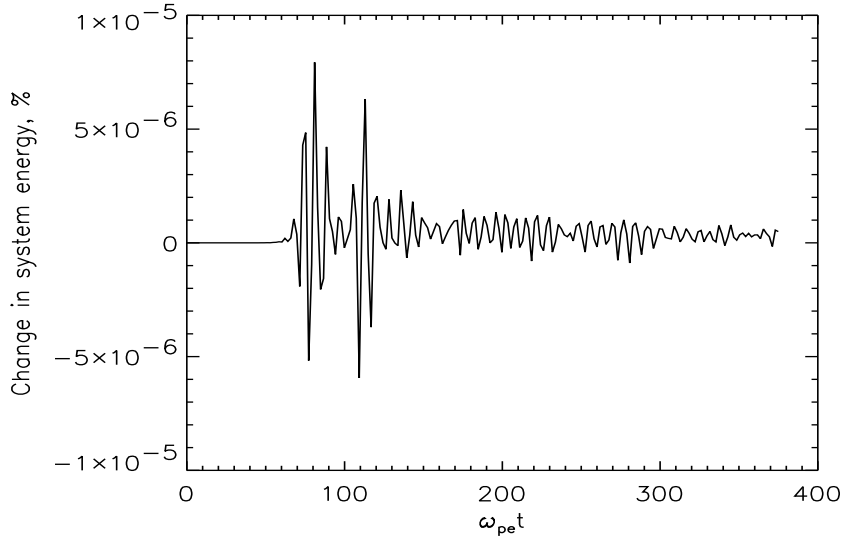

Figure 3.10: *Percentage change in the total system energy during the gentle-bump simulation run.*

and the particle energy density of each plasma species is given by:

$$K_\alpha(t) = \int m_\alpha v_z^2 f_{\alpha 0}(v_z, t) dv_z \tag{3.31}$$

where $f_{\alpha 0}(v_z, t)$ denotes the spatially-averaged distribution function. Figure 3.10 shows the percentage change in total energy density $T_E = W_E + K_e + K_i$ throughout the simulation, where the change was calculated in the same manner as in Eq. (3.29). As with the previous check, the percentage change in energy density is oscillatory after an initial period, this time after $\sim 50\omega_{pe}^{-1}$. The percentage change in energy density is much smaller than the percentage change in I_e, the largest difference being $8 \times 10^{-6}\%$. This shows that the Vlasov code conserves the total energy density very well.

Finally, the last check is for the conservation of particle momentum. The waves in the simulation are electrostatic, and therefore cannot change their momentum via wave-particle interactions [*Swanson,* p.294, 1989]. Instead we concentrate on the particles. Their momentum is given by:

$$p_\alpha = \int m_\alpha v_z f_{\alpha 0}(v_z, t) dv_z \tag{3.32}$$

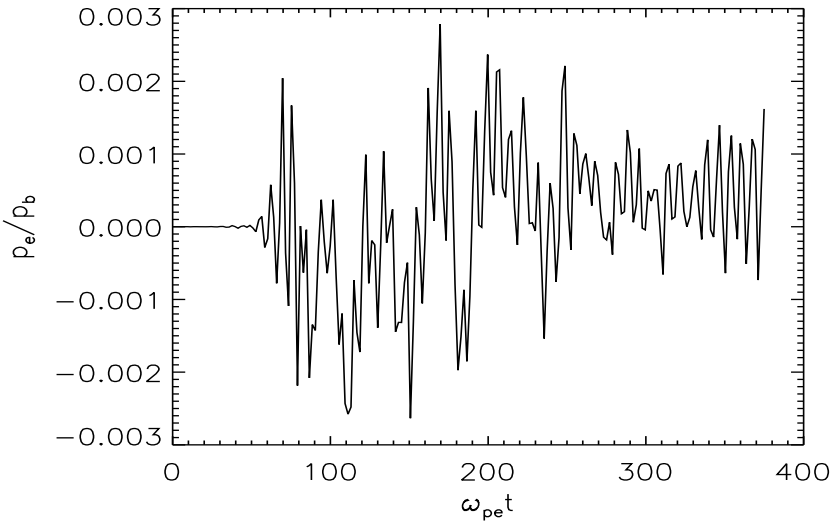

Figure 3.11: *Evolution of the electron momentum during the gentle-bump simulation run, normalized to the beam momentum.*

Figure 3.11 shows the total particle momentum throughout the simulation normalized by the initial momentum of one of the beams p_b. This normalization is merely to illustrate the relative size of the changes in total particle momentum. The original particle momentum is exactly zero, since the two beams traveling through the stationary bulk plasma distribution have equal and opposite beam velocities. Again, the change in particle momentum is oscillatory after $\sim 35\omega_{pe}^{-1}$, but instead of oscillating around zero, the average particle momentum appears to be less than zero for $80\omega_{pe}^{-1} < t < 160\omega_{pe}^{-1}$ and more than zero for $t > 250\omega_{pe}^{-1}$. However, these relatively small changes in total momentum throughout the simulation are not physically damaging, and the system still behaves as expected (see discussion in previous section).

References

Akasofu, S.-I., A note on the Chapman-Ferraro theory, in *Physics of the Magnetopause, Geophysical Monograph, 90,* edited by P. Song, B. U. Ö. Sonnerup and M. F. Thomsen, American Geophysical Union, Washington D.C., 1995.

Akimoto, K., and D. Winske, Ion-acoustic-like waves excited by the reflected ions at the Earth's Bow Shock, *Journal of Geophysical Research, 90,* 12095-12103, 1985.

Anderson Jr., J. D., Discretization of Partial Differential Equations, in *An Introduction to Computational Fluid Dynamics*, edited by J. F. Wendt, p. 83-100, Springer-Verlag, 1992.

Anderson, R. R., G. K. Parks, T. E. Eastman, D. A. Gurnett, and L. A. Frank, Plasma waves associated with energetic particles streaming into the solar wind from the Earth's Bow Shock, *Journal of Geophysical Research, 86,* 4493-4510, 1981.

Anderson, R. R., C. C. Harvey, M. M. Hoppe, B. T. Tsurutani, T. E. Eastman, and J. Etcheto, Plasma waves near the magnetopause, *Journal of Geophysical Research, 87,* 2087-2107, 1982.

Appert, K., and J. Vaclavik, Tail formation by nonresonant interaction of ions with ion-acoustic turbulence, *Plasma Physics, 23,* 763-774, 1981.

Arnoldy, R. L., Signature in the interplanetary medium for substorms, *Journal of Geophysical Research, 76,* 5189-5201, 1971.

Baum, P. J., A. Bratenahl, M. Kao, and R. S. White, Plasma instability at an X-type neutral point, *Physics of Fluids, 16,* 1501-1504, 1973.

Berchem, J., and C. T. Russell, The thickness of the magnetopause current layer: ISEE1 and 2 observations, *Journal of Geophysical Research, 87,* 2108-2114, 1982.

Berman, R. H., D. J. Tetreault, T. H. Dupree, and T. Boutros-Ghali, Computer simulation of nonlinear ion-electron instability, *Physical Review Letters, 48,* 1249-1252, 1982.

Biermann, L., Kometshweife und solare Korpuskularstrahlung, *Zeitscrift für Astrophysik, 29,* 274, 1951.

Birk, G. T., and A. Otto, Consequences of a resistive instability operating in the upper auroral ionosphere, *Journal of Atmospheric and Solar-Terrestrial Physics, 59,* 835-847, 1997.

Birkeland, K., *The Norwegian Aurora Polaris Expedition, 1902-3,* p1-315, H. Aschehoug, Christiana, Norway, 1908.

Birn, J., J. F. Drake, M. A. Shay, B. N. Rodgers, R. E. Denton, M. Hesse, M. Kuznetsova, Z. W. Ma, A. Bhattarcharjee, A. Otto, and P. L. Pritchett, Geospace Environmental Modeling (GEM) magnetic reconnection challenge, *Journal of Geophysical Research, 106,* 3715-3719, 2001.

Birn, J., and M. Hesse, Geospace Environment Modeling (GEM) magnetic reconnection challenge: resistive tearing, anisotropic pressure and Hall effects, *Journal of Geophysical Research, 106,* 3737-3750, 2001.

Biskamp, D., On conventional and unconventional theory of ion sound turbulence, *Nuclear Fusion, 12,* 85-87, 1972.

Biskamp, D., and R. Chodura, Computer simulation of anomalous resistance, *Proceedings of the Fourth International Conference on Plasma Physics and Controlled Nuclear Fusion Research,* International Atomic Energy Agency, Vienna, 1971a.

Biskamp, D., and R. Chodura, Computer simulation of anomalous dc resistivity, *Physical Review Letters, 27,* 1553-1556, 1971b.

Biskamp, D., K. U. Von Hegenow, and H. Welter, Computer studies of current-driven ion-sound turbulence in three dimensions, *Physics Letters, 39A,* 351-352, 1972.

Biskamp, D., and R. Chodura, Collisionless dissipation of a cross-field electric current, *Physics of Fluids, 16,* 893-901, 1973.

Biskamp, D. E. Schwarz, and J. F. Drake, Two-fluid theory of collisionless magnetic reconnection, *Physics of Plasmas, 4,* 1002-1009, 1997.

Bittencourt, J. A., *Fundamentals of Plasma Physics,* Pergamon Press Ltd., Oxford, UK, 1986.

Bonetti, A., H. S. Bridge, A. J. Lazarus, B. Rossi, and F. Scherb, Explorer 10 plasma measurements, *Journal of Geophysical Research, 68,* 4017-4063, 1963.

Bratenahl, A., and C. M. Yeates, Experimental study of magnetic flux transfer at the hyperbolic neutral point, *Physics of Fluids, 13,* 2696-2709, 1970.

Caan, M. N., R. L. McPherron, and C. T. Russell, Solar wind and substorm-related changes in the lobes of the geomagnetic tail, *Journal of Geophysical Research, 78,* 8087-8093, 1973.

Califano, F. and M. Lontano, Vlasov-Poisson Simulations of Strong Wave-Plasma Interaction in Conditions of Relevance for Radio Frequency Plasma Heating, *Physical Review Letters, 83*, 96-99, 1999.

Carlson, C.W., J. P. McFadden, R. E. Ergun, M. Temerin, W. Peria, F. S. Mozer, D. M. Klumpar, E. G. Shelley, W. K. Peterson, E. Moebius, R. Elphic, R. Strangeway, C. Cattell, R. Pfaff, FAST observations in the downward auroral current region: Energetic upgoing electron beams, parallel potential drops, and ion heating, *Geophysical Research Letters, 25,* 2017-2020, 1998.

Cattell, C. A., F. S. Mozer, I. Roth, R. R. Anderson, R. C. Elphic, W. Lennartsson, and E. Ungstrup, ISEE1 observations of electrostatic ion cyclotron waves in association with ion beams on auroral field lines from ~ 2.5 to 4.5 R_E, *Journal of Geophysical Research, 96,* 11421-11439, 1991.

Chanteur, G., Vlasov Simulations of Ion Acoustic Double Layers, in *Computer Simulation of Space Plasmas*, edited by H. Matsumoto and T. Sato, pp 279-301, Terra Scientific, Tokyo, 1984.

Chapman, S., and V. C. A. Ferraro, A new theory of magnetic storms, Part 1, The initial phase, *Terrestrial Magnetism and Atmospheric Electricity, 36,* 7, 1931.

Chaston, C. C., Y. D. Hu and B. J. Fraser, Quasi-linear ion cyclotron heating in the near-Earth magnetotail, *Journal of Geophysical Research, 105,* 5507-5516, 2000.

Choueiri, E. Y., Anomalous resistivity and heating in current-driven plasma thrusters, *Physics of Fluids, 6,* 2290-2306, 1999.

Christon, S. P., D. J. Williams, D. G. Mitchell, L. A. Frank and C. Y. Huang, Spectral characteristics of plasma sheet ion and electron populations during disturbed geomagnetic conditions, *Journal of Geophysical Research, 94,* 13409-13424, 1989.

Chust, T., P. Louarn, M. Volwerk, H. de Feraudy, A. Roux, J. E. Wahlund, B. Holback, Electric fields with a large parallel component observed by the Freja spacecraft: Artifacts or real signals, *Journal of Geophysical Research, 103,* 215-224, 1998.

Coleman, I. J., G. Chisham, M. Pinnock, and M. P. Freeman, An ionospheric convection signature of antiparallel reconnection, *Journal of Geophysical Research, in press,* 2001.

Collis, P. N., I. Häggström, K. Kaila, and M. T. Rietveld, EISCAT radar observations of enhanced incoherent scatter spectra; their relation to red aurora and field-aligned currents, *Geophysical Research Letters, 18,* 1031-1034, 1991.

Coroniti, F. V., and C. F. Kennel, Polarization of the auroral electrojet, *Journal of Geophysical Research, 78,* 2835, 1972.

Coroniti, F. V., and A. Eviatar, Magnetic field reconnection in a collisionless plasma, *Astrophysical Journal Supplement Series, 33,* 189-210, 1977.

Cowley, S. W. H., Comments on the merging of non-antiparallel magnetic fields, *Journal of Geophysical Research, 81,* 3455-3458, 1976.

Cowley, S. W. H., Magnetic Reconnection, in *Solar System Magnetic Fields,* edited by E. R. Priest, pp121-155, Dordrecht, 1985.

Cowley, S. W. H., and C. J. Owen, A simple illustrative model of open flux tube motion over the dayside magnetopause, *Planetary and Space Science, 37,* 1461-1475, 1989.

Cravens, T. E., *Physics of Solar System Plasmas,* Cambridge University Press, Cambridge, UK, 1997.

Crooker, N. U., Dayside merging and cusp geometry, *Journal of Geophysical Research, 96,* 951-959, 1979.

Davidson, R. C., N. A. Krall, K. Papadopoulos and R. Shanny, Electron heating by electron-ion beam instabilities, *Physical Review Letters, 24,* 579-582, 1970.

Davidson, R. C., and N. T. Gladd, Anomalous transport properties associated with the lower-hybrid-drift instability, *Physics of Fluids, 18,* 1327-1335, 1975.

deAgua, L. B., Y. Omura, H. Matsumoto, and A. L. Brinca, Competing processes of plasma wave instabilities driven by an anisotropic electron beam: Linear results and two-dimensional particle simulations, *Journal of Geophysical Research, 101,* 15475-15490, 1996.

Dendy, R. O., *Plasma Dynamics,* Oxford University Press, Oxford, UK, 1990.

Deng, X. H., and H. Matsumoto, Rapid magnetic reconnection in the Earth's magnetosphere mediated by whistler waves, *Nature, 410,* 557-580, 2001.

Drake, J. F., Magnetic Reconnection: A kinetic treatment, in *Physics of the Magnetopause,* Geophysical Monograph 90, edited by P. Song, B. U. Ö. Sonnerup and M. F. Thomsen, American Geophysical Union, Washington, DC, 1995.

Dum, C. T., R. Chodura, and D. Biskamp, Turbulent heating and quenching of the ion sound instability, *Physical Review Letters, 32,* 1231-1234, 1974.

Dungey, J. W., Interplanetary magnetic field and the auroral zones, *Physical Review Letters, 6,* 47-48, 1961.

Dupree, T. H., Growth of phase-space density holes, *Physics of Fluids, 26,* 2460-2481, 1983.

Elphic, R. C., and S. P. Gary, ISEE observations of low-frequency waves and ion distribution function evolution in the plasma sheet boundary layer, *Geophysical Research Letters, 17,* 2023-2026, 1990.

Escoubet, C. P., R. Schmidt, and M. L. Goldstein (Eds.), Cluster - Science and mission overview, *Space Science Reviews, 79,* Nos. 1-2, 1997.

Etemadi, A., S. W. H. Cowley, M. Lockwood, B. J. I. Bromage, D. M. Willis, and H. Luhr, The dependence of high-latitude ionospheric flows on the North-South component of the IMF: a high time resolution correlation analysis using EISCAT Polar and AMPTE-UKS and IRM data, *Planetary and Space Science, 36,* 471-498, 1988.

Fairfield, D. H., and L. J. Cahill Jr., Transition region magnetic field and polar magnetic disturbances, *Journal of Geophysical Research, 71,* 155-169, 1966.

Fairfield, D, H, and N. F. Ness, Configuration of the geomagnetic tail during substorms, *Journal of Geophysical Research, 75,* 7032-7047, 1970.

Feldman, W. C., R. C. Anderson, S. J. Bame, S. P. Gary, J. T. Gosling, D. J. McComas and M. F. Thomsen, Electron Velocity Distributions Near the Earth's Bow Shock, *Journal of Geophysical Research, 88*, 96-110, 1983.

Fijalkow, E., A numerical solution to the Vlasov equation, *Computer Physics Communications, 116*, 319-328, 1999.

Forme, F. R. E., D. Fontaine, and J.-E. Wahlund, Two different types of enhanced ion acoustic fluctuations observed in the upper ionosphere, *Journal of Geophysical Research, 100,* 14625-14636, 1995.

Formisano, V., and R. Torbert, Ion acoustic wave forms generated by ion-ion streams at the Earth's bow shock, *Geophysical Research Letters, 9,* 207-210, 1982.

Forslund, D., R. Morse, and C. Nielson, Theory of turbulent heating and anomalous diffusion in pinch plasmas, *Proceedings of the Fourth International Conference on Plasma Physics and Controlled Nuclear Fusion Research,* International Atomic Energy Agency, Vienna, 1971.

Foster, J. C., C. del Pozo, K. Groves, J.-P. St.-Maurice, Radar observations of the onset of current driven instabilities in the topside ionosphere, *Geophysical Research Letters, 15,* 160-163, 1988.

Frank, L. A., W. R. Paterson and M. G. Kivelson, Observations of nonadiabatic

acceleration of ions in Earth's magnetotail, *Journal of Geophysical Research, 99,* 14877-14890, 1994.

Fried, B. D., and S. D. Conte, *The Plasma Dispersion Function,* Academic Press, New York, 1961.

Fuselier, S. A., and D. A. Gurnett, Short-wavelength ion waves upstream of the Earth's bow shock, *Journal of Geophysical Research, 89,* 91-103, 1984.

Fuselier, S. A., S. P. Gary, M. F. Thomsen, S. J. Bame and D. A. Gurnett, Ion beams and the ion/ion acoustic instability upstream from the Earth's bow shock, *Journal of Geophysical Research, 92,* 4740-4744, 1987.

Galeev, A. A., and R. Z. Sagdeev, Current instabilities and anomalous resistivity of plasmas, in *Basic Plasma Physics, Vol II,* edited by A. A. Galeev and R. N. Sudan, pp271-303, North-Holland Physics Publishing, Amsterdam, The Netherlands, 1984.

Gallagher, D. L., Short-wavelength electrostatic waves in the earth's magnetosheath, *Journal of Geophysical Research, 90,* 1435-1448, 1985.

Gary, S. P., Plasma instabilities in the terrestrial magnetosphere: a review of recent theoretical research, *Physica Scripta, T18,* 179-187, 1987.

Gary, S. P., *Theory of Space Microinstabilities,* Cambridge University Press, Cambridge, UK, 1993.

Gosling, J. T., J. R. Asbridge, S. J. Bame, W. C. Feldman, G. Paschmann, N. Sckopke, and C. T. Russell, Evidence for quasi-stationary reconnection at the dayside magnetopause, *Journal of Geophysical Research, 87,* 2147-2158, 1982.

Gosling, J. T., M. F. Thomsen, S. J. Bame, R. C. Elphic, and C. T. Russell, Plasma flow reversals at the dayside magnetopause and the origin of asymmetric polar cap convection, *Journal of Geophysical Research, 95,* 8073-8084, 1990.

Gosling, J. T., M. F. Thomsen, S. J. Bame, R. C. Elphic, and C. T. Russell, Observations of reconnection of interplanetary and lobe magnetic field lines at the high-latitude magnetopause, *Journal of Geophysical Research, 96,* 14097-14106, 1991.

Grabbe, C. L., and T. E. Eastman, Generation of broadband electrostatic noise by ion beam instabilities in the magnetotail, *Journal of Geophysical Research, 89,* 3865, 1984.

Greenwald, R. A., K. Baker, J. M. Ruohoniemi, J. R. Dudeney, M. Pinnock, N. Mattin, and J. M. Leonard, Simultaneous conjugate observations of dynamic variations in high-latitude dayside convection due to changes in IMF B_y, *Journal of*

Geophysical Research, 95, 8057-8072, 1990.

Gurnett, D. A., and L. A. Frank, Ion acoustic waves in the solar wind, *Journal of Geophysical Research, 83,* 58-68, 1978.

Gurnett, D. A., E. Marsch, W. Pilipp, R. Schwenn and H. Rosenbauer, Ion-acoustic waves and related plasma observations in the solar wind, *Journal of Geophysical Research, 84*, 2029-2038, 1979a.

Gurnett, D. A., R. R. Anderson, B. T. Tsurutani, E. J. Smith, G. Paschmann, G. Haerendel, S. J. Bame, and C. T. Russell, Plasma wave turbulence at the magnetopause, observations from ISEE1 and 2, *Journal of Geophysical Research, 84,* 7043-7058, 1979b.

Haerendel, G., G. Paschmann, N. Sckopke, H. Rosenbauer, and P. C. Hedgecock, The frontside boundary layer of the magnetopause and the problem of reconnection, *Journal of Geophysical Research, 83,* 3195-3216, 1978.

Hess, R. A., R. J. MacDowell, B. Goldstein, M. Neugebauer, and R. J. Forsyth, Ion acoustic-like waves observed by Ulysses near interplanetary shock waves in the three-dimensional heliosphere, *Journal of Geophysical Research, 103,* 6531-6541, 1998.

Hesse, M., J. Birn, and M. Kuznetsova, Collisionless magnetic reconnection: electron processes and transport modelling, *Journal of Geophysical Research, 106,* 3721-3735, 2001.

Hockney, R. W., and J. W. Eastwood, *Computer Simulation Using Particles,* Institute of Physics Publishing, London, UK, 1988.

Hoffmeister, C., Physikalisch Untersuchungen auf Kometen I, Die Beziehungen des primaren Schweifstrahl zum Radius vektor, *Zeitschrift für Astrophysik, 22,* 265-285, 1943.

Horiuchi, R. and T. Sato, Three-dimensional particle simulation of plasma instabilities and collisionless reconnection in a current sheet, *Physics of Plasmas, 6*, 4565-4574, 1999

Horne, R. B. and M. P. Freeman, A New Electrostatic Simulation Code by Numerical Integration of the Vlasov and Ampère Equations using MacCormack's Method, *Journal of Computational Physics, 171,* 182-200, 2001.

Horton, W., Ion acoustic turbulence and anomalous transport, *Journal of Statistical Physics, 39,* 739-754, 1985.

Ichimaru, S., *Basic Principles of Plasma Physics: A Statistical Approach*,

Addison-Wesley, Reading, Massachussets, 1973.

Kelley, M. C., F. S. Mozer, and U. V. Fahleson, Measurements of the electric field component of waves in the auroral ionosphere, *Planetary and Space Science, 18,* 847, 1970.

Kennel, C. F., F. L. Scarf, F. V. Coroniti, E. J. Smith, and D. A. Gurnett, Nonlocal plasma turbulence associated with interplanetary shocks, *Journal of Geophysical Research, 87,* 17-34, 1982.

Kessel, R. L., S.-H. Chen. J. L. Green, S. F. Fung, S. A. Boardsen, L. C. Tan, T. E. Eastman, J. D. Craven, and L. A. Frank, Evidence of high-latitude reconnecting during northward IMF: Hawkeye observations, *Geophysical Research Letters, 23,* 583-586, 1996.

Kindel, J. M., and C. F. Kennel, Topside current instabilities, *Journal of Geophysical Research, 76,* 3055-3078, 1971.

Klimas, A. J., A method for overcoming the velocity space filamentation problem in collisionless plasma model solutions, *Journal of Computational Physics, 68,* 202-226, 1987.

Krall, N. A., and A. W. Trivelpiece, *Principles of Plasma Physics,* McGraw-Hill, Inc., New York, 1973.

Kurth, W. S., D. A. Gurnett, and F. L. Scarf, High-resolution spectrograms of ion acoustic waves in the solar wind, *Journal of Geophysical Research, 84,* 3413-3419, 1979.

Kuznetsova, M. M., M. Hesse, and D. Winske, Collisionless reconnection supported by nongyrotropic pressure effects in hybrid and particle simulations, *Journal of Geophysical Research, 106,* 3799-3810, 2001.

Labelle, J., R. A. Treumann, G. Haerendel, O. H. Bauer, G. Paschmann, W. Baumjohann, H. Luhr, R. R. Anderson, H. C. Koons, and R. H. Holzworth, AMPTE-IRM observations of waves associated with flux transfer events in the magnetosphere, *Journal of Geophysical Research, 92,* 5827-5843, 1987.

Labelle, J., and R. A. Treumann, Plasma waves at the dayside magnetopause, *Space Science Reviews, 47,* 175-202, 1988.

Landau, L. D., On the vibrations of the electronic plasma, *Journal of Physics (Academy of Sciences of the U.S.S.R.), 10,* 25, 1946.

Lester, M., M. Lockwood, T. K. Yeoman, S. W. H. Cowley, H. Luhr, R. Bunting, and C. J. Farrugia, The response of ionospheric convection in the polar-cap to

substorm activity, *Annales Geophysicae, 13,* 147-158, 1995.

Lindman, E., Numerical simulation of ion-acoustic turbulence, *Journal of Statistical Physics, 39,* 769-782, 1985.

Lockwood, M., Solar Wind-Magnetospheric Coupling, in *Incoherent Scatter: Theory, Practice and Science,* edited by D. Alcayde, Technical Report 97/53, EISCAT Scientific Association, Kiruna, 1997.

Lui, A. T. Y., A synthesis of magnetospheric substorm models, *Journal of Geophysical Research, 96,* 1849-1856, 1991.

Lui, A. T. Y., P. H. Yoon and C. L. Chang, Quasi-linear analysis of ion Weibel instability in the Earth's neutral sheet, *Journal of Geophysical Research, 98,* 153-163, 1993.

Lysak, R. L., and T. Dum, Dynamics of magnetosphere-ionosphere coupling including turbulent transport, *Journal of Geophysical Research, 88,* 365-380, 1983.

Ma, Z. W., and A. Bhattarcharjee, Hall magnetohydrodynamic reconnection: The Geospace Environment Modeling challenge, *Journal of Geophysical Research, 106,* 3773-3782, 2001.

Malmberg, J. H., and C. B. Wharton, Collisionless damping of large-amplitude plasma waves, *Physical Review Letters, 19,* 775-777, 1967.

Matsumoto, H. and K. Fukuchi, Computer-simulation of particle-acceleration and wave excitation by electron-beam injection from space-shuttle, *Geophysical Research Letters, 12,* 61-64, 1985.

Matsumoto, H., H. Kojima, T. Miyatake, Y. Omura, M. Okada, I. Nagano, and M. Tsutsui, Electrostatic solitary waves (ESW) in the magnetotail - BEN wave-forms observed by Geotail, *Geophysical Research Letters, 21,* 2915-2918, 1994.

Maunder, E. W., Magnetic disturbances, 1882 to 1903, as recorded at the Royal Observatory, Greenwich, and their association with sunspots, *Monthly Notices of the Royal Astronomical Society, 65,* 2, 1905.

McFadden, J. P., C. W. Carlson, and R. E. Ergun, Microstructure of the auroral acceleration region as observed by FAST, *Journal of Geophysical Research, 104,* 14453-14480, 1999.

McPherron, R. L., C. T. Russell, and M. Aubry, Satellite studies of magnetospheric substorms on August 15, 1968, 9. Phenomenological model for substorms, *Journal of Geophysical Research, 78,* 3131-3149, 1973.

McPherron, R. L., Physical processes producing magnetospheric substorms and magnetic storms, in *Geomagnetism, Vol. 4,* edited by J. A. Jacobs, Academic Press Limited, London, UK, 1991.

Miyake, T., Y. Omura, H. Matsumoto, and H. Kojima, Two-dimensional computer simulations of electrostatic solitary waves observed by Geotail spacecraft, *Journal of Geophysical Research, 103,* 11841-11850, 1998.

Miyake, T., Y. Omura, and H. Matsumoto, Electrostatic particle simulations of solitary waves in the auroral region, *Journal of Geophysical Research, 105,* 23239-23249, 2000.

Montgomery, M. D., J. R. Asbridge and S. J. Bame, Vela 4 plasma observations near the Earth's bow shock, *Journal of Geophysical Research, 75,* 1217-1231, 1970.

Morse, R. L., and C. W. Nielson, Numerical simulation of a warm two-beam plasma, *Physics of Fluids, 12,* 2418-2425, 1969.

Mozer, F. S., and P. Bruston, Electric field measurements in the auroral ionosphere, *Journal of Geophysical Research, 72,* 1109-1114, 1967.

Nishida, A., and N. Nagayama, Synoptic survey for the neutral line in the magnetotail during the substorm expansion phase, *Journal of Geophysical Research, 78,* 3782-3798, 1973.

Nunn, D., Y. Omura, H. Matsumoto, I. Nagano and S. Yagitani, The numerical simulation of VLF chorus and discrete emissions observed on the Geotail satellite using a Vlasov code, *Journal of Geophysical Research, 102,* 27083-27097, 1997.

O'Neil, T., Collisionless damping of nonlinear plasma oscillations, *Physics of Fluids, 8,* 2255-2262, 1965.

Ogilvie, K. W., R. J. Fitzenreiter and J. D. Scudder, Observations of electron beams in the low-latitude boundary-layer, *Journal of Geophysical Research, 89,* 10723-10732, 1984.

Øieroset, M., T. D. Phan, M. Fujimoto, R. P. Lin, and R. P. Lepping, In situ detection of collisionless reconnection in the Earth's magnetotail, *Nature, 412,* 414-416, 2001.

Omura, Y., H. Kojima, and H. Matsumoto, Computer-simulation of electrostatic solitary waves - a nonlinear model of broad-band electrostatic noise, *Geophysical Research Letters, 21,* 2923-2926, 1994.

Omura, Y., and H. Matsumoto, KEMPO1: Technical Guide to One-dimensional Electromagnetic Particle Code, in *Computer Space Plasma Physics: Simulation*

Techniques and Software, edited by H. Matsumoto and Y. Omura, Terra Scientific Publishing Company, Tokyo, Japan, 1993.

Omura, Y., H. Matsumoto, T. Miyake and H. Kojima, Electron beam instabilities as generation mechanism of electrostatic solitary waves in the magnetotail, *Journal of Geophysical Research, 101,* 2685-2697, 1996.

Otto, A., Geospace Environment Modeling (GEM) magnetic reconnection challenge: MHD and Hall-MHD - constant and current dependent resistivity models, *Journal of Geophysical Research, 106,* 3751-3757, 2001.

Ozaki, M., T. Sato, R. Horiuchi and the Complexity Simulation Group, Electromagnetic instability and anomalous resistivity in a magnetic neutral sheet, *Physics of Plasmas, 3*, 2265-2274, 1996.

Papadopoulos, K., A review of anomalous resistivity for the ionosphere, *Reviews of Geophysics and Space Physics, 15,* 113-127, 1977.

Parker, E., Dynamics of the interplanetary gas and magnetic fields, *Astrophysical Journal, 128,* 664-676, 1958.

Parker, E. N., The solar-flare phenomenon and the theory of reconnection and annihilation of magnetic fields, *Astrophysical Journal Supplement Series, 8,* 177-212, 1963.

Paschmann, G., I. Papamastorakis, N. Sckopke, B. U. Ö. Sonnerup, S. J. Bame, and C. T. Russell, ISEE observations of the magnetopause - reconnection and the energy-balance, *Journal of Geophysical Research, 90,* 12111-12120, 1985.

Paschmann, G., I. Papamastorakis, W. Baumjohann, N. Sckopke, C. W. Carlson, B. U. Ö. Sonnerup, and H. Luhr, The magnetopause for large magnetic shear - AMPTE/IRM observations, *Journal of Geophysical Research, 91,* 11099-11115, 1986.

Perreault, P., and S.-I. Akasofu, A study of geomagnetic storms, *Geophysical Journal of the Royal Astronomical Society, 54,* 547-473, 1978.

Petschek, H. E., Magnetic field annihilation, in *AAS-NASA Symposium on the Physics of Solar Flares,* NASA Special Publication SP-50, 425, 1964.

Pilipenko, V. A., S. L. Shalimov, E. N. Federov, M. J. Engebretson, and W. J. Hughes, Coupling between field-aligned current impulses and Pi1 noise bursts, *Journal of Geophysical Research, 104,* 17419-17430, 1999.

Pritchett, P. L., Geospace Environment Modeling magnetic reconnection challenge: Simulations with a full particle electromagnetic code, *Journal of Geophysical*

Research, 106, 3783-3798, 2001.

Rietveld, M. T., P. N. Collis, and J.-P. St.-Maurice, Naturally enhanced ion acoustic waves in the auroral ionosphere observed with the EISCAT-933 MHz radar, *Journal of Geophysical Research, 96,* 19291-19305, 1991.

Rishbeth, H., P. R. Smith, S. W. H. Cowley, D. M. Willis, A. P. van Eyken, B. J. I. Bromage and S. R. Crothers, Ionospheric response to changes in the interplanetary magnetic field observed by EISCAT and AMPTE-UKS, *Nature, 318,* 451-452, 1985.

Rodriguez, P., and D. A. Gurnett, Correlation of bow shock plasma wave turbulence with solar wind parameters, *Journal of Geophysical Research, 80,* 19, 1975.

Rostoker, G., and C.-G. Fälthammer, Relationship between changes in the interplanetary magnetic field and variations in the magnetic field at the earth's surface, *Journal of Geophysical Research, 72,* 5853, 1967.

Rostoker, G., Some observational constraints for substorm models, in *Magnetospheric Substorms,* Geophysical Monograph 64, edited by J. R. Kan, T. A. Potemra, S. Kokubun, and T. Iijima, American Geophysical Union, Washington, DC, 1991a.

Rostoker, G., Auroral signatures of magnetospheric substorms and constraints which they provide for substorm theories, *Journal of Geomagnetism and Geoelectricity, 43,* 233-243, Part 1, Suppl. S, 1991b.

Russell, C. T., and R. C. Elphic, ISEE observations of flux transfer events at the dayside magnetopause, *Geophysical Research Letters, 6,* 33-36, 1979.

Šafránková, J., Z. Němeček, D. G. Sibeck, L. Přech, J. Měrka, and O. Santolík. Two point observation of high-latitude reconnection, *Geophysical Research Letters, 25,* 4301-4304, 1998.

Sagdeev, R. Z., On Ohm's Law resulting from instability, in *Proceedings of a Symposium in Applied Mathematics of the American Mathematical Society,* edited by H. Grad, 281-286, American Mathematical Society, Providence, Rhode Island, 1967.

Sato, T., and H. Okuda, Numerical simulations on ion acoustic double-layers, *Journal of Geophysical Research, 86,* 3357-3368, 1981.

Scarf, F. L., R. W. Fredricks, L. A. Frank, C. T. Russell, P. J. Coleman, Jr., and M. Neugebauer, Direct correlations of large-amplitude waves with suprathermal protons in the upstream solar wind, *Journal of Geophysical Research, 75,* 7316-7322, 1970.

Scarf, F. L., F. V. Coroniti, C. F. Kennel, E. J. Smith, J. A. Slavin, B. T. Tsurutani,

S. J. Bame, and W. C. Feldman, Plasma wave spectra near slow mode shocks in the distant magnetotail, *Geophysical Research Letters, 11,* 1050-1053, 1984.

Scarf, F. L., F. V. Coroniti, C. F. Kennel, D. A. Gurnett, W.-H. Ip, and E. J. Smith, Plasma wave observations at comet Giacobini-Zinner, *Science, 232,* 377-379, 1986.

Schumer, J. W. and J. P. Holloway, Vlasov Simulations using Velocity-Scaled Hermite Representations, *Journal of Computational Physics, 144*, 626-661, 1998.

Scudder, J. D., D. L. Lind and R. W. Ogilvie, Electron observations in the solar wind and the magnetosheath, *Journal of Geophysical Research, 78,* 6535-6548, 1973.

Scurry, L., C. T. Russell, and J. T. Gosling, A statistical study of accelerated flow events at the dayside magnetopause, *Journal of Geophysical Research, 99,* 14815-14829, 1994.

Sedgemore-Schulthess, K. J. F., M. Lockwood, T. S. Trondsen, B. S. Lanchester, M. H. Rees, D. A. Lorentzen, and J. Moen, Coherent EISCAT Svalbard Radar spectra from the dayside cusp-cleft and their implications for transient field-aligned currents, *Journal of Geophysical Research, 104,* 24613-24624, 1999.

Shatten, K. H., and J. M. Wilcox, Response of the geomagnetic activity index K_p to the interplanetary magnetic field, *Journal of Geophysical Research, 72,* 5185, 1967.

Shay, M. A., J. F. Drake, R. E. Denton, and D. Biskamp, Structure of the dissipation region during collisionless magnetic reconnection, *Journal of Geophysical Research, 103,* 9165-9176, 1998.

Shay, M. A., J. F. Drake, B. N. Rogers, and R. E. Denton, Alfvénic collisionless magnetic reconnection and the Hall term, *Journal of Geophysical Research, 106,* 3759-3772, 2001.

Singh, N., Computer experiments on the formation and dynamics of electric double layers, *Plasma Physics, 22,* 1, 1980.

Song, P., Observations of waves at the dayside magnetopause, in *Solar wind sources of magnetospheric ultra-low frequency waves, AGU Monograph, 81,* edited by M. Engebretson, K. Tazahashi, and M. Scholer, 159-171, 1994.

Sonnerup, B. U. Ö., Theory of the low-latitude boundary layer, *Journal of Geophysical Research, 85,* 2017-2026, 1980.

Sonnerup, B. U. Ö., G. Paschmann, I. Papmastorakis, N. Sckopke, G. Haerendel, S. J. Bame, J. R. Asbridge, J. T. Gosling and C. T. Russell, Evidence for magnetic-field reconnection at the Earth's magnetopause, *Journal of Geophysical Research, 86,* 10049-10067, 1981.

Stenzel, R. L., W. Gekelman, and N. Wild, Double layer formation during current sheet disruptions in a reconnection experiment, *Geophysical Research Letters, 9,* 680-683, 1982.

Stix, T. H., *Waves in Plasmas,* American Institute of Physics, New York, 1992.

Swanson, D. G., *Plasma Waves*, Academic Press, Inc., San Diego, CA, 1989.

Sweet, P. A., The neutral point theory of solar flares, in *Electromagnetic Phenomena in Cosmical Physics,* edited by B. Lehnert, 123-134, Cambridge University Press, London, UK, 1958.

Swift, D. W., A mechanism for energizing electrons in the magnetosphere, *Journal of Geophysical Research, 70,* 3061-3073, 1965.

Temerin, M., K. Cerny, W. Lotko, and F. S. Mozer, Observations of double layers and solitary waves in the auroral plasma, *Physical Review Letters, 48,* 1175-1179, 1982.

Todd, H., S. W. H. Cowley, M. Lockwood, D. M. Willis, and H. Luhr, Response time of the high-latitude dayside ionosphere to sudden changes in the North-South component of the IMF, *Planetary and Space Science, 36,* 1415-1428, 1988.

Toida, M., T. Maeda, I. Shiiba, A. Sugishima, and Y. Ohsawa, Simulation studies of heavy ion heating by current-driven instabilities, *Physics of Plasmas, 7,* 4882-4888, 2000.

Treumann, R. A., J. Labelle, and R. Pottelette, Plasma diffusion at the magnetopause: The case of lower hybrid drift waves, *Journal of Geophysical Research, 96,* 16009-16013, 1991.

Treumann, R. A., and W. Baumjohann, *Basic Space Plasma Physics*, Imperial College Press, London, 1996.

Treumann, R. A., and W. Baumjohann, *Advanced Space Plasma Physics*, Imperial College Press, London, 1997.

Tsurutani, B. T., E. J. Smith, R. M. Thorne, R. R. Anderson, D. A. Gurnett, G. K. Parks, C. S. Lin, and C. T. Russell, Wave-particle interactions at the magnetopause: contributions to the dayside aurora, *Geophysical Research Letters, 8,* 183-186, 1981.

Tsurutani, B. T., A. L. Brinca, E. J. Smith, R. T. Okida, R. R. Anderson, and T. E. Eastman, A statistical study of ELF-VLF plasma waves at the magnetopause, *Journal of Geophysical Research, 94,* 1270-1280, 1989.

Usui, H., H. Matsumoto, and Y. Omura, Plasma response to high-potential satellite

in electrodynamic tether system, *Journal of Geophysical Research, 98,* 1531-1544, 1993.

Vasyliunas, V. M., Theoretical models of magnetic field line merging, 1, *Reviews of Geophysics and Space Physics, 13,* 303-336, 1975.

Wahlund, J.-E., F. R. E. Forme, H. J. Opgenoorth, M. A. L. Persson, E. V. Mishin, and A. S. Volokitin, Scattering of electromagnetic waves from a plasma: enhanced ion acoustic fluctuations due to ion-ion two-stream instabilities, *Geophysical Research Letters, 19,* 1919-1922, 1992.

Wahlund, J.-E., P. Louarn, T. Chust, H. de Feraudy, A. Roux, B. Holback, P.-O. Dovner, and G. Holmgren, On ion acoustic turbulence and the nonlinear evolution of kinetic Alfvén waves in aurora, *Geophysical Research Letters, 21,* 1831-1834, 1994.

Wahlund, J.-E., P. Louarn, T. Chust, H. de Feraudy, A. Roux, B. Holback, B. Cabrit, A. I. Eriksson, P. M. Kintner, M. C. Kelley, J. Bonnell, and S. Chesney, Observations of ion acoustic fluctuations in the auroral topside ionosphere by the Freja S/C, *Geophysical Research Letters, 21,* 1835-1838, 1994.

Wahlund, J.-E., A. I. Eriksson, B. Holback, M. H. Boehm, J. Bonnell, P. M. Kintner, C. E. Seyler, J. H. Clemmons, L. Eliasson, D. J. Knudsen, P. Norqvist, and L. J. Zanetti, Broadband ELF plasma emission during auroral energization 1. Slow ion acoustic waves, *Journal of Geophysical Research, 103,* 4343-4375, 1998.

Wang, J. G., D. L. Newman and M. V. Goldman, Vlasov simulations of electron heating by Langmuir turbulence near the critical altitude in the radiation-modified ionosphere, *Journal of Atmospheric and Solar-Terrestrial Physics, 59,* 2461-2474, 1997.

Wharton, C. B., J. H. Malmberg and T. M. O'Neil, Nonlinear effects of large-amplitude plasma waves, *Physics of Fluids, 11,* 1761-1763, 1968.

Wiegelmann, T., and J. Büchner, Evolution of magnetic helicity in the course of kinetic magnetic reconnection, Nonlinear Processes in Geophysics, in press, 2001.

Winske, D., V. A. Thomas and N. Omidi, Diffusion at the magnetopause: a theoretical perspective, in *Physics of the Magnetopause,* Geophysical Monograph 90, edited by P. Song, B. U. Ö. Sonnerup and M. F. Thomsen, American Geophysical Union, Washington, DC, 1995.

Yagatani, S., I. Nagano, Y. Omura and H. Matsumoto, Comparison between particle simulation and full-wave analysis for wave-propagation in a nonuniform plasma, *Radio Science, 27,* 449-462, 1992.

Yin, L., M. Ashour-Abdalla, R. L. Richard, L. A. Frank and W. R. Paterson,

Generation of electrostatic waves by discontinuous electron distributions, *Journal of Geophysical Research, 104,* 12415-12429, 1999.

Yoon, P. H., Plasma heating by a purely growing mode driven by cross-field currents in quasiperpendicular collisionless shock, *Physics of Fluids, 3,* 3074-3081, 1991.

Yoon, P. H., C. S. Wu and M. E. Mandt, Ion heating by kinetic cross-field streaming instability due to reflected ions at a quasiperpendicular shock, *Physics of Fluids, 4,* 719-729, 1992.

Zhang, Y. L., H. Matsumoto, and Y. Omura, Linear and nonlinear interactions of an electron-beam with oblique whistler and electrostatic waves in the magnetosphere, *Journal of Geophysical Research, 98,* 21353-21363, 1993.